

Fast Electrons Interacting with Chiral Matter: Mirror-Symmetry Breaking of Quantum Decoherence and Lateral Momentum Transfer

A. Ciattoni^{ID*}

CNR-SPIN, c/o Dip.to di Scienze Fisiche e Chimiche, Via Vetoio, Coppito, L'Aquila 67100, Italy



(Received 11 April 2022; revised 4 January 2023; accepted 27 February 2023; published 27 March 2023)

Photons experience mirror asymmetry of macroscopic chiral media, as in circular dichroism and polarization rotation, since left- and right-handed circular polarizations differently couple with matter handedness. Conversely, free relativistic electrons with vanishing orbital angular momentum have no handedness so the question arises whether they can sense chirality of geometrically symmetric macroscopic samples. In this paper, we show that matter chirality breaks mirror symmetry of the scattered electrons' quantum decoherence, even when the incident electron wave function and the sample shape have a common reflection symmetry plane. This is physically possible since the wave-function transverse smearing triggers electron sensitivity to the spatial asymmetry of the electromagnetic interaction with the sample, as results from our nonperturbative analysis of the scattered electron reduced density matrix, in the framework of macroscopic quantum electrodynamics. Furthermore, we prove that mirror asymmetry also shows up in the distribution of the electron lateral momentum, orthogonal to the geometric symmetry plane, whose nonvanishing mean value reveals that the electron experiences a lateral mechanical interaction entirely produced by matter chirality.

DOI: 10.1103/PhysRevApplied.19.034086

I. INTRODUCTION

Molecular chirality is an important topic in science both for its implications in chemistry, biology, and medicine and for the physical effects produced by microscopic mirror-symmetry breaking. The coupling of a chiral molecule with the electromagnetic field involves both its electric and magnetic dipoles [1] whose combined polar and axial characters trigger molecular sensitivity to radiation handedness, a property routinely used to detect chirality by means of circular dichroism and polarization rotation [2]. The large mismatch between molecular size and wavelength both makes such effects very small and establishes the dipolar interaction which forbids the molecule to sense the spatial variations of the field. However, macroscopic chiral samples with a large number of chiral molecules display macroscopic mirror-symmetry breaking and consequently support chiroptical effects driven by the symmetry of the spatial field profile, such as the suppression of field mirror symmetry upon reflection by chiral molecular films (mirror optical activity) [3,4], or the antenna emission of asymmetric fields in chiral metamaterials [5]. Tight subwavelength confinement of the field reduces the molecule-field spatial scale mismatch and accordingly it enhances the above chiroptical spatial effects, analogously to other chiral nanophotonic phenomena [6–10].

The ability of electron microscopes to focus the beam down to the subnanometer scale makes fast electrons an ideal continuum source of ultraconfined electromagnetic field [11] whose evanescent character can in principle be used to enhance spatially asymmetric chiroptical effects, this leading to indirect chiral sensing by detecting the diffraction radiation from a lateral nanostructure [3]. On the other hand, apart from specific diffraction techniques where a transmission electron microscope is used to identify chirality at atomic scale [12,13], only a few methods have been proposed to directly sense chirality of non-crystalline samples containing chiral molecules in electron microscopes. Magnetically induced chirality can be probed by comparing electron energy-loss spectra taken in opposite magnetic fields and under suitable electron scattering conditions (electron energy-loss magnetic chiral dichroism) [14,15]. In the nonmagnetic case, the idea of a probing electron with a handedness able to sense matter chirality has led to consideration of electron vortex beams [16,17] carrying orbital angular momentum whose exchange with the sample has been shown to provide chiral information in both elastic scattering from crystals [18,19] and inelastic scattering from plasmonic samples with chiral shape and single chiral molecules [20]. A different approach based on the photon-induced near-field electron microscopy technique [21–23] has been proposed [24] where the probing handedness is injected by means of circularly polarized radiation and the chirality of the plasmonic sample shape

* alessandro.ciattoni@spin.cnr.it

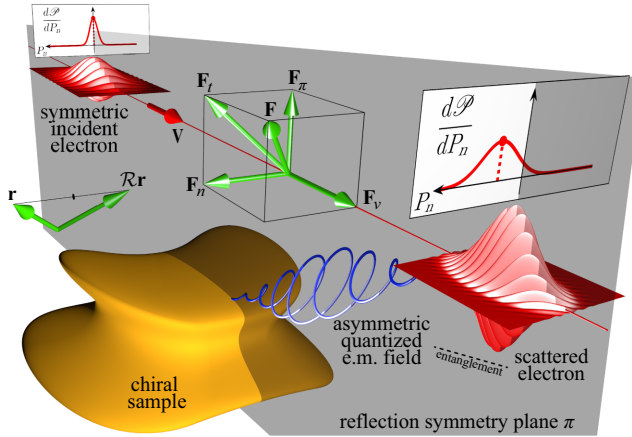


FIG. 1. Scattering setup. The shape of the chiral sample has a reflection symmetry plane π (\mathcal{R} is reflection through π) and the incident electron wave function is mirror-symmetric with its velocity V lying on π . The scattered electron is entangled with the spatially asymmetric quantized electromagnetic field mediating its interaction with the sample, this producing mirror-symmetry breaking of electron decoherence. \mathbf{F}_v and \mathbf{F}_t are the parts of a vector \mathbf{F} parallel and orthogonal to V , while \mathbf{F}_π and \mathbf{F}_n are the parts of \mathbf{F}_t parallel and orthogonal to π . The distribution $d\mathcal{P}/dP_n$ of the lateral momentum P_n of the scattered electron is not symmetric, unlike that of the incident electron.

is retrieved from the spatial scan of the electron energy spectrum.

In this paper, we show that a fast electron with initial mirror-symmetric wave function (i.e., with no handedness) does experience microscopic chirality of a symmetrically shaped macroscopic sample (see Fig. 1): the quantum decoherence of the scattered electron turns out to be mirror-asymmetric due to a chiroptical spatial effect generalizing mirror optical activity. To this end, we evaluate the nonperturbative reduced density matrix of the scattered electron by using macroscopic quantum electrodynamics [25–28], an appropriate framework for dealing with the electron-sample entanglement [29–31] which is ultimately responsible for electron decoherence [32–36]. Besides, by using the density matrix, we show that the distribution of the momentum component orthogonal to the reflection symmetry plane (see Fig. 1) is not mirror-symmetric, thus showing that the scattered electron gains a net lateral momentum purely due to the sample chirality. We specialize our general discussion to an aloof electron probing a realistic chiral nanofilm where the above asymmetric effects are magnified by the relatively long effective interaction length.

II. INTERACTION OF A FAST ELECTRON WITH A MACROSCOPIC CHIRAL SAMPLE

Macroscopic quantum electrodynamics (MQED) provides the description of the quantized field coupled to

the chiral sample via the spectral electric field $\hat{\mathbf{E}}_\omega(\mathbf{r}) = \sum_\lambda \int d^3\mathbf{r}' \mathcal{G}_{\omega\lambda}(\mathbf{r}, \mathbf{r}') \hat{\mathbf{f}}_{\omega\lambda}(\mathbf{r}')$ and Hamiltonian $\hat{H}_{\text{em}} = \int_0^\infty d\omega \hbar \omega \sum_\lambda \int d^3\mathbf{r} \hat{\mathbf{f}}_{\omega\lambda}^\dagger(\mathbf{r}) \cdot \hat{\mathbf{f}}_{\omega\lambda}(\mathbf{r})$, where $\hat{\mathbf{f}}_{\omega\lambda}(\mathbf{r}) \cdot \mathbf{e}_j$ is the annihilation operator of a polaritonic excitation of frequency ω and type $\lambda = e, m$ (electric and magnetic) at position \mathbf{r} and in direction j , whereas $\mathcal{G}_{\omega\lambda}(\mathbf{r}, \mathbf{r}')$ are two tensors related to the sample Green's tensor $\mathcal{G}_\omega(\mathbf{r}, \mathbf{r}')$ [27] which fully captures the electromagnetic response of the sample. In turn it satisfies the inhomogeneous Helmholtz equation

$$\left\{ \nabla \times \frac{1}{\mu} \nabla \times -\frac{\omega^2}{c^2} \left(\epsilon - \frac{\kappa^2}{\mu} \right) + \frac{\omega}{c} \left[\left(\nabla \frac{\kappa}{\mu} \right) \times + 2 \frac{\kappa}{\mu} \nabla \times \right] \right\} \mathcal{G}_\omega(\mathbf{r}, \mathbf{r}') = \delta(\mathbf{r} - \mathbf{r}') I \quad (1)$$

where $\epsilon(\mathbf{r}, \omega)$, $\mu(\mathbf{r}, \omega)$, and $\kappa(\mathbf{r}, \omega)$ are the medium permittivity, permeability, and chiral parameter, respectively (see Appendix A for a detailed summary of MQED in chiral media).

The electron is assumed to be almost monoenergetic and highly directional, with its momentum \mathbf{P} slightly differing from a reference momentum \mathbf{P}_0 so that, as discussed in Appendix B, its Hamiltonian in paraxial and nonrecoil approximations is $\hat{H}_{\text{el}} = \mathbf{V} \cdot \hat{\mathbf{P}}$, where $\mathbf{V} = c\mathbf{P}_0/\sqrt{m^2c^2 + P_0^2}$ and $\hat{\mathbf{P}}$ are the electron velocity and momentum operator. In the same approximation, the chiral sample-electron interaction Hamiltonian is $\hat{H}_{\text{int}} = e[\mathbf{V} \cdot \hat{\mathbf{A}}(\hat{\mathbf{R}}) - \hat{\Phi}(\hat{\mathbf{R}})]$, where $-e < 0$ and $\hat{\mathbf{R}}$ are the electron charge and position operator, while $\hat{\mathbf{A}}$ and $\hat{\Phi}$ are the vector and scalar potential operators in the Coulomb gauge related to the transverse and longitudinal parts of the electric field operator. Time evolution produced by the Hamiltonian $\hat{H}_{\text{em}} + \hat{H}_{\text{el}} + \hat{H}_{\text{int}}$ can be analytically dealt with, analogously to the achiral situation [37], and the rigorous scattering operator \hat{S} we have obtained is detailed in Appendix B. The incident electron wave function is

$$\psi_i(\mathbf{R}) = \frac{1}{\sqrt{\ell}} \phi_i(\mathbf{R}_t) e^{i(E_i/\hbar V) R_v}, \quad (2)$$

where subscripts v and t henceforth label the parts of a vector parallel and orthogonal to V (see Fig. 1), ϕ_i is the initial transverse wave-function profile, E_i is the initial electron energy, and ℓ is the longitudinal quantization length. Since no radiation is initially involved in the scattering setup we are considering, the initial electron-field state is $|\Psi_i\rangle = |\psi_i\rangle \otimes |0\rangle$, where $|0\rangle$ is the polaritonic vacuum state. The final state $|\Psi\rangle = \hat{S}|\Psi_i\rangle$ displays electron-field entanglement, resulting from processes of electron energy loss and multipolariton excitation of any order, so that measurement predictions about the electron (with the field

left unmeasured) have to be performed by resorting to the reduced density operator $\hat{\rho}_e = \text{Tr}_{\text{Fock}} |\Psi\rangle \langle \Psi|$ where the trace is taken over the polariton Fock space. In the position representation, we get the reduced density matrix

$$\rho_e(\mathbf{R}, \mathbf{R}') = \psi_i(\mathbf{R}) \psi_i^*(\mathbf{R}') \gamma(\mathbf{R}, \mathbf{R}') \quad (3)$$

(see Appendix C for the detailed derivation), where

$$\gamma(\mathbf{R}, \mathbf{R}') = e^{i[\Phi(\mathbf{R}_t) - \Phi(\mathbf{R}'_t)] - (1/2)[\Delta(\mathbf{R}_t, \mathbf{R}_t) + \Delta(\mathbf{R}'_t, \mathbf{R}'_t)]} e^{\Delta(\mathbf{R}, \mathbf{R}')} \quad (4)$$

is the decoherence factor of the scattered electron with

$$\begin{aligned} \Phi(\mathbf{R}_t) &= \frac{4\alpha}{c} \int_0^{+\infty} d\omega \int_{-\infty}^{+\infty} dq \\ &\times \int_{-\infty}^q dq' \sin\left[\frac{\omega}{V}(q - q')\right] \\ &\times \text{Im} [\mathbf{u}_v \cdot \mathcal{G}_\omega(\mathbf{R}_t + qu_v, \mathbf{R}_t + q'u_v) \mathbf{u}_v], \quad (5) \\ \Delta(\mathbf{R}, \mathbf{R}') &= \frac{4\alpha}{c} \int_0^\infty d\omega e^{-i(\omega/V)(R_v - R'_v)} \\ &\times \int_{-\infty}^{+\infty} dq \int_{-\infty}^{+\infty} dq' e^{i(\omega/V)(q - q')} \\ &\times \text{Im} [\mathbf{u}_v \cdot \mathcal{G}_\omega(\mathbf{R}_t + qu_v, \mathbf{R}'_t + q'u_v) \mathbf{u}_v], \end{aligned}$$

in which α is the fine-structure constant and $\mathbf{u}_v = \mathbf{V}/V$ is the velocity unit vector. The first exponential on the right-hand side of Eq. (4) physically arises from elastic processes due to the zero-point fluctuations of the field, while the second exponential containing $\Delta(\mathbf{R}, \mathbf{R}')$ provides the inelastic contribution to electron decoherence, standard mechanisms in achiral environments [38,39] that we have generalized here in the presence of chiral matter.

From the above reduced density matrix it is possible to evaluate the transverse momentum distribution

$$\begin{aligned} \frac{d\mathcal{P}}{d^2\mathbf{P}_t} &= \frac{1}{(2\pi\hbar)^2} \int d^2\mathbf{R}_t \int d^2\mathbf{R}'_t e^{-(i/\hbar)\mathbf{P}_t \cdot (\mathbf{R}_t - \mathbf{R}'_t)} \\ &\times \phi_i(\mathbf{R}_t) \phi_i^*(\mathbf{R}'_t) \gamma(\mathbf{R}_t, \mathbf{R}'_t) \quad (6) \end{aligned}$$

and its mean value

$$\begin{aligned} \langle \mathbf{P}_t \rangle &= \int d^2\mathbf{R}_t \phi_i^* \left(\frac{\hbar}{i} \nabla_{\mathbf{R}_t} \right) \phi_i \\ &+ \int d^2\mathbf{R}_t |\phi_i|^2 \left[\frac{\hbar}{i} \nabla_{\mathbf{R}_t} \log \gamma(\mathbf{R}_t, \mathbf{R}'_t) \right]_{\mathbf{R}'_t=\mathbf{R}_t}, \quad (7) \end{aligned}$$

as detailed in Appendix D.

III. MIRROR ASYMMETRY OF ELECTRON DECOHERENCE AND LATERAL MOMENTUM TRANSFER

The above expressions for the reduced density matrix and transverse momentum distribution are rather general with regard to their dependence on the Green's tensor, formally holding also for achiral media. On the other hand, medium chirality has an impact on the Green's tensor behavior under spatial reflections, a topic we discuss here as a prelude to the investigation of the mirror-symmetry breaking of the electron quantum properties. To this end, with reference to Fig. 1, we consider the geometric spatial reflection $\mathbf{r}^M = \mathcal{R}\mathbf{r}$ through an arbitrary mirror plane π , where $\mathcal{R} = I - 2\mathbf{n}\mathbf{n}$ is the reflection tensor and \mathbf{n} is the unit vector normal to π . In order to avoid geometrical mirror asymmetries, we henceforth focus on a geometrically mirror-symmetric medium for which $\varepsilon(\mathcal{R}\mathbf{r}, \omega) = \varepsilon(\mathbf{r}, \omega)$, $\mu(\mathcal{R}\mathbf{r}, \omega) = \mu(\mathbf{r}, \omega)$, and $\kappa(\mathcal{R}\mathbf{r}, \omega) = \kappa(\mathbf{r}, \omega)$. Now it is simple to prove that the mirror image of the Green's tensor $\mathcal{G}_\omega^M(\mathbf{r}, \mathbf{r}') = \mathcal{R}\mathcal{G}_\omega(\mathcal{R}\mathbf{r}, \mathcal{R}\mathbf{r}')\mathcal{R}$ satisfies the equation

$$\begin{aligned} &\left\{ \nabla \times \frac{1}{\mu} \nabla \times -\frac{\omega^2}{c^2} \left(\varepsilon - \frac{\kappa^2}{\mu} \right) \right. \\ &\left. + \frac{\omega}{c} \left[\left(\nabla \frac{-\kappa}{\mu} \right) \times + 2 \frac{-\kappa}{\mu} \nabla \times \right] \right\} \mathcal{G}_\omega^M(\mathbf{r}, \mathbf{r}') \\ &= \delta(\mathbf{r} - \mathbf{r}') I \quad (8) \end{aligned}$$

which is identical to Eq. (1) except for the sign switch of the chirality parameter κ . In other words, $\mathcal{G}_\omega^M(\mathbf{r}, \mathbf{r}')$ is the Green's tensor of the opposite enantiomeric medium which is the mirror image of the original one (since microscopically each chiral molecule is reflected into its opposite enantiomer). This observation is a mere restatement of reflection invariance (or mirror symmetry) of classical electrodynamics which states that if a complete experiment (i.e., field, sources, and matter) is subjected to mirror reflection, the resulting experiment should, in principle, be realizable. What is remarkable here is that reflection invariance additionally entails the mirror asymmetry of the Green's tensor of a chiral medium,

$$\mathcal{R}\mathcal{G}_\omega(\mathcal{R}\mathbf{r}, \mathcal{R}\mathbf{r}')\mathcal{R} \neq \mathcal{G}_\omega(\mathbf{r}, \mathbf{r}'), \quad (9)$$

which is an evident consequence of the incompatibility of Eqs. (8) and (1) with the assumption that $\mathcal{G}_\omega^M(\mathbf{r}, \mathbf{r}') = \mathcal{G}_\omega(\mathbf{r}, \mathbf{r}')$. Evidently in an achiral medium where $\kappa = 0$, Eqs. (8) and (1) coincide so that, by uniqueness of solutions, $\mathcal{G}_\omega^M(\mathbf{r}, \mathbf{r}') = \mathcal{G}_\omega(\mathbf{r}, \mathbf{r}')$, that is, the Green's tensor is mirror-symmetric.

Mirror-symmetry breaking of the electron quantum properties is a consequence of the Green's tensor mirror asymmetry. In order to discuss such effects we here

consider an electron whose velocity \mathbf{V} lies on the sample symmetry plane π (see Fig. 1) and whose initial wave function is left invariant by \mathcal{R} , i.e.,

$$\phi_i(\mathcal{R}\mathbf{R}_t) = \phi_i(\mathbf{R}_t). \quad (10)$$

The reflection \mathcal{R} considered, when acting on a vector \mathbf{F} , does not affect its part parallel to the electron velocity, that is, $\mathcal{R}\mathbf{F}_v = \mathbf{F}_v$. In addition, since the transverse part \mathbf{F}_t lies in the plane orthogonal to π , it can be decomposed as $\mathbf{F}_t = \mathbf{F}_\pi + \mathbf{F}_n$, where

$$\begin{aligned} \mathbf{F}_\pi &= \frac{1}{2} (\mathbf{F}_t + \mathcal{R}\mathbf{F}_t), \\ \mathbf{F}_n &= \frac{1}{2} (\mathbf{F}_t - \mathcal{R}\mathbf{F}_t) \end{aligned} \quad (11)$$

are its parts parallel (π) and orthogonal (n) to the reflection plane π (see Fig. 1). We refer to \mathbf{F}_n as the lateral part of the vector \mathbf{F} . The chosen configuration is geometrically mirror-symmetric and the occurrence of any mirror-symmetry breaking is accordingly of pure physical origin and due to the medium chirality. Since $\mathcal{R}\mathbf{u}_v = \mathbf{u}_v$, Eq. (9) readily yields $\mathbf{u}_v \cdot \mathcal{G}_\omega(\mathcal{R}\mathbf{r}, \mathcal{R}\mathbf{r}') \mathbf{u}_v \neq \mathbf{u}_v \cdot \mathcal{G}_\omega(\mathbf{r}, \mathbf{r}') \mathbf{u}_v$ which, combined with Eqs. (5), directly implies that $\Phi(\mathcal{R}\mathbf{R}_t) \neq \Phi(\mathbf{R}_t)$, and $\Delta(\mathcal{R}\mathbf{R}, \mathcal{R}\mathbf{R}') \neq \Delta(\mathbf{R}, \mathbf{R}')$ so that, from Eq. (4), we eventually get

$$\gamma(\mathcal{R}\mathbf{R}, \mathcal{R}\mathbf{R}') \neq \gamma(\mathbf{R}, \mathbf{R}'). \quad (12)$$

This proves that the mirror symmetry of the electron quantum decoherence is broken by medium chirality, and this is one of the main result of this paper. The reduced density matrix [see Eq. (3)] of the scattered electron is therefore mirror-asymmetric as well, except for a fully localized initial electron, $|\phi_i(\mathbf{R}_t)|^2 = \delta(\mathbf{R}_t)$, since in this case the relevant decoherence factor is $\gamma(\mathbf{R}_v, \mathbf{R}'_v)$ which is evidently mirror-symmetric. Mirror-symmetry breaking of the reduced density matrix can be physically grasped by noting that the chiral sample, when exposed to the symmetric field produced by the bare electron, produces a mirror-asymmetric field through a mechanism generalizing mirror optical activity of chiral films [3]. Such reaction field self-consistently acts back on the electron and its spatial asymmetry is conveyed to the reduced density matrix if the electron wave function has a transverse smearing, since a pointlike particle lying on the symmetry plane π cannot sense the spatial asymmetry of the field.

Equation (12) directly implies that the transverse momentum distribution in Eq. (6) is not left invariant by the transverse momentum reflection $\mathbf{P}_t \rightarrow \mathcal{R}\mathbf{P}_t$. As a consequence, using the decomposition $\mathbf{P}_t = \mathbf{P}_\pi + \mathbf{P}_n$ [see Eqs. (11)], we obtain the result that the lateral momentum distribution of the scattered electron, $d\mathcal{P}/dP_n =$

$\int dP_\pi d\mathcal{P}/d^2\mathbf{P}_t$ (since $d^2\mathbf{P}_t = dP_n dP_\pi$), is not symmetric in P_n , unlike that of the incident electron (see Fig. 1) which is symmetric by reflection invariance of ϕ_i . Accordingly, the scattered electron has a nonvanishing lateral momentum mean value which, from Eqs. (7) and (11), is given by

$$\langle \mathbf{P}_n \rangle = \frac{1}{2} \int d^2\mathbf{R}_t |\phi_i|^2 \left[\frac{\hbar}{i} \nabla_{\mathbf{R}_t} \log \frac{\gamma(\mathbf{R}_t, \mathbf{R}'_t)}{\gamma(\mathcal{R}\mathbf{R}_t, \mathcal{R}\mathbf{R}'_t)} \right]_{\mathbf{R}'_t=\mathbf{R}_t}, \quad (13)$$

dramatically showing that it is entirely due to matter chirality by means of the mirror asymmetry of the decoherence factor [see Eq. (12)]. Such lateral momentum transfer testifies that the electron is subjected to a mechanical interaction orthogonal to π which is geometrically analogous to, but physically different from, the optical lateral force experienced by chiral nanoparticles [40,41]. As a final general remark we stress that the global spatial mirror symmetry of the sample we have hitherto considered (see Fig. 1) is not strictly required to observe the lateral momentum transfer predicted in Eq. (13). This is due to the fact that sample spatial mirror symmetry is evidently required only over the very small region surrounding the electron trajectory where the quantum field ruling electron-chiral film interaction is practically nonvanishing.

IV. ALOOF ELECTRON TRAVELING PARALLEL TO A CHIRAL FILM

To discuss our general results in a realistic situation, we consider the setup sketched in Fig. 2(a) where an aloof electron travels in a vacuum ($\epsilon_1 = 1$) with velocity $\mathbf{V} = V\mathbf{e}_x$ parallel to a homogeneous chiral nanofilm of thickness $d = 50$ nm and deposited onto a substrate ($\epsilon_2 = 1.48$), assuming infinite extension along the y axis and finite length L along the x axis. We assume an elliptical Gaussian transverse profile for the initial wave function, $\phi_i(Y, Z) = \sqrt{2/\pi\sigma_y\sigma_z} e^{-\{(Y^2/\sigma_y^2)+(Z+b)^2/\sigma_z^2\}}$, of widths σ_y and σ_z and impact parameter b . In Fig. 2(b) we plot the nanofilm permittivity ϵ and chiral parameter κ modeling typical chiral molecules with ultraviolet resonance at 3.54 eV embedded in a dielectric matrix, with negligible magnetic response ($\mu = 1$) [42]. Such a maximally symmetric setup has $\pi = zx$ as its reflection symmetry plane so that, from the comparison of Figs. 1 and 2(a), we get $\mathcal{R} = \mathbf{e}_x\mathbf{e}_x - \mathbf{e}_y\mathbf{e}_y + \mathbf{e}_z\mathbf{e}_z$, $\mathbf{F}_v = F_x\mathbf{e}_x$, $\mathbf{F}_\pi = F_z\mathbf{e}_z$, and $\mathbf{F}_n = F_y\mathbf{e}_y$; asymmetric effects accordingly show up along the y axis, which is the lateral direction.

In order to evaluate the decoherence factor $\gamma(\mathbf{R}, \mathbf{R}')$ of the scattered electron in Eq. (4), the Green's tensor component along the electron velocity $\mathbf{e}_x \cdot \mathcal{G}_\omega(\mathbf{r}, \mathbf{r}') \mathbf{e}_x = \mathcal{G}_{\omega xx}(\mathbf{r}, \mathbf{r}')$ in a vacuum ($z < 0$, $z' < 0$) is required and its analytical evaluation is enabled by plane geometry, as

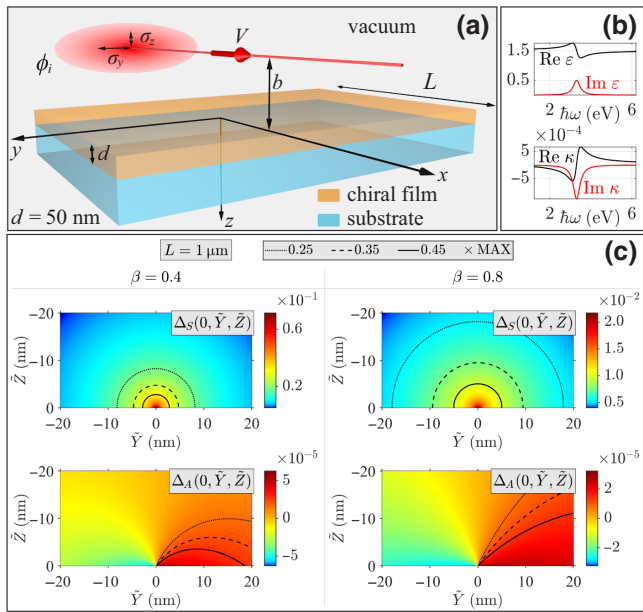
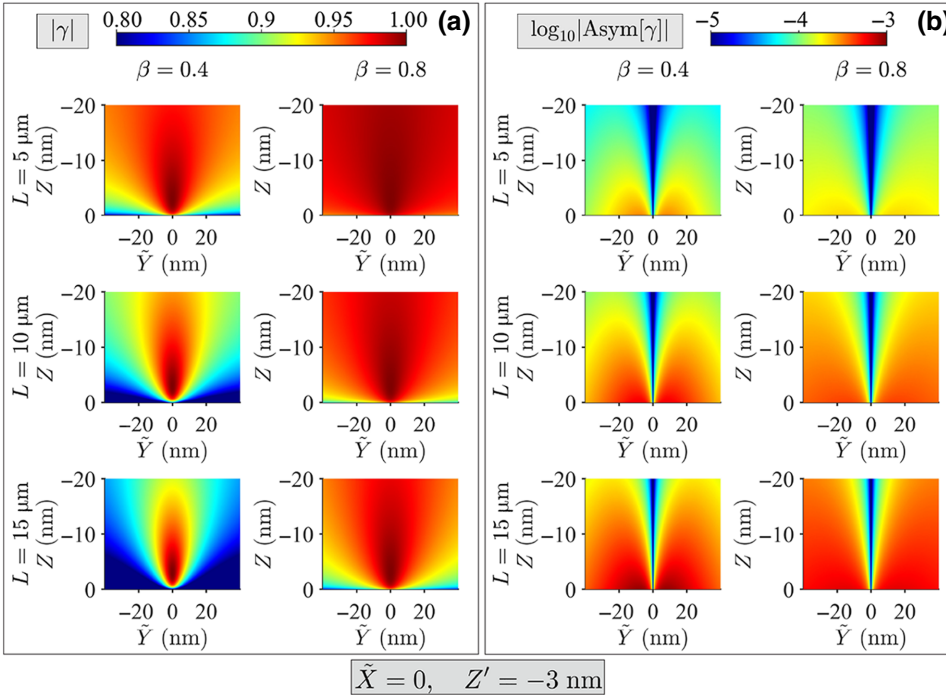


FIG. 2. (a) Scattering of an aloof electron by a chiral nanofilm deposited on a substrate. (b) Film permittivity ϵ and chiral parameter κ . (c) Symmetric and antisymmetric parts of Δ for two electron velocities $\beta = V/c$ (columns). For graphical clarity purposes, suitable level curves are plotted as dotted, dashed, and solid black lines.

detailed in Appendix E where we also prove that it displays mirror asymmetry [in agreement with the general Eq. (9)] as a consequence of mirror optical activity discussed in [3,4]. After inserting $\mathcal{G}_{\omega xx}$ into Eqs. (5), we obtain



the phase factor $\Phi(Z)$, which is irrelevant in our symmetry analysis since it only depends on Z , together with the fundamental quantity

$$\Delta(\mathbf{R}, \mathbf{R}') = \Delta_S(\tilde{X}, \tilde{Y}, \tilde{Z}) + i\Delta_A(\tilde{X}, \tilde{Y}, \tilde{Z}) \quad (14)$$

where we have set $\tilde{X} = X - X'$, $\tilde{Y} = Y - Y'$, $\tilde{Z} = Z + Z'$ and where the real quantities Δ_S and Δ_A are reported in Eqs. (F9) of Appendix F. Remarkably, Δ_S and Δ_A are proportional to the interaction length L and are respectively symmetric and antisymmetric under the lateral reflection $\tilde{Y} \rightarrow -\tilde{Y}$:

$$\begin{aligned} \Delta_S(\tilde{X}, -\tilde{Y}, \tilde{Z}) &= \Delta_S(\tilde{X}, \tilde{Y}, \tilde{Z}), \\ \Delta_A(\tilde{X}, -\tilde{Y}, \tilde{Z}) &= -\Delta_A(\tilde{X}, \tilde{Y}, \tilde{Z}). \end{aligned} \quad (15)$$

All the electron mirror-symmetry breaking effects are a consequence of Δ_A which evidently vanishes in the achiral limit $\kappa \rightarrow 0$. In Fig. 2(c) we plot Δ_S and Δ_A at $\tilde{X} = 0$ and $\tilde{Z} < 0$ (vacuum) for the interaction length $L = 1 \mu\text{m}$, for two electron velocities. Their relevant features are a consequence of the fact that the electron velocity selects the photon momentum $k_x = -\omega/V$ which entails the fully evanescent character of the field and the corresponding enhancement of the film chiral response. At lower electron velocities such evanescent character is more pronounced, since the photon momentum parallel to the film is $\sqrt{(\omega/V)^2 + k_y^2}$, and accordingly both Δ_S and Δ_A are boosted, showing tighter spatial confinement and larger amplitudes.

FIG. 3. Moduli of (a) the scattered electron decoherence factor $\gamma(\tilde{X}, \tilde{Y}, Z, Z')$ and (b) its asymmetry degree $\text{Asym}[\gamma](\tilde{X}, \tilde{Y}, Z + Z')$ for $\tilde{X} = 0$ and $Z' = -3 \text{ nm}$ and for various electron velocities $\beta = V/c$ (columns) and interaction lengths L (rows). For lower electron velocities and larger interaction lengths the electron-sample coupling is magnified and accordingly the spatial spot of $|\gamma|$ (localized around Z') shrinks and its asymmetry $|\text{Asym}[\gamma]|$ is more pronounced.

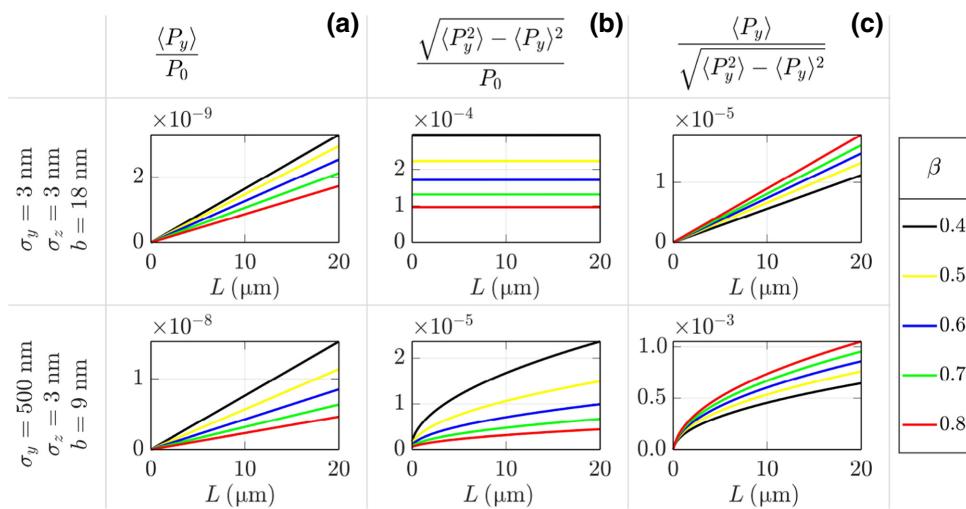


FIG. 4. Dependence of the lateral momentum transfer on the interaction length L and electron velocity $\beta = V/c$ (colors) for two incident electron configurations: a tightly confined and distant electron (first row) and a laterally wider and closer one (second row). (a) Mean value and (b) root-mean-square of the lateral momentum P_y gained by the scattered electron, normalized with the reference momentum $P_0 = mV/\sqrt{1 - (V/c)^2}$. They are both larger at longer L and lower β . The wider and closer electron (second row) experiences larger lateral momentum gain. Lateral momentum transfer efficiency (c) (peak factor) is larger for the wider and closer electron (second row).

In Fig. 3 we display the scattered electron decoherence factor $\gamma(\tilde{X}, \tilde{Y}, Z, Z')$ and its mirror-symmetry breaking for various interaction lengths L and two electron velocities, for $\tilde{X} = 0$ and $Z' = -3$ nm. The modulus of γ in Fig. 3(a) turns out to be localized around the chosen reference Z' , and its spatial spread, for a fixed interaction length, is smaller at lower electron velocities, as a consequence of the evanescent mechanism ruling Δ discussed in Fig. 2. In addition, the spatial spot of γ shrinks considerably at larger interaction lengths, for a fixed electron velocity, an effect resulting from the nonperturbative character of the decoherence factor in Eq. (4) and testifying that first-order perturbation theory is not adequate in the setup considered here for interaction lengths of the order of tens of micrometers. In Fig. 3(b) we plot the modulus of the mirror-asymmetry degree of the decoherence factor, defined as

$$\text{Asym}[\gamma(\mathbf{R}, \mathbf{R}')] = 2 \frac{\gamma(\mathbf{R}, \mathbf{R}') - \gamma(\mathcal{R}\mathbf{R}, \mathcal{R}\mathbf{R}')}{\gamma(\mathbf{R}, \mathbf{R}') + \gamma(\mathcal{R}\mathbf{R}, \mathcal{R}\mathbf{R}')}, \quad (16)$$

which, using Eq. (4), turns out to be

$$\text{Asym}[\gamma] = 2i \tan \Delta_A. \quad (17)$$

Mirror asymmetry of the decoherence factor is again more pronounced at lower electron velocities owing to the above-discussed behavior of Δ_A and it increases considerably at larger interaction lengths.

In Fig. 4 we display the dependence of the overall phenomenology concerning lateral momentum transfer on the interaction length and the electron velocity, for two

initial electron configurations: a tightly confined and distant electron with $(\sigma_y, \sigma_z, b) = (3, 3, 18)$ nm (first row) and a laterally wider and closer one with $(\sigma_y, \sigma_z, b) = (500, 3, 9)$ nm (second row). In Figs. 4(a) and 4(b) we respectively plot the mean value $\langle P_y \rangle$ and root-mean-

square $\sqrt{\langle P_y^2 \rangle - \langle P_y \rangle^2}$ (see Appendix F) of the electron lateral momentum [both normalized with the reference momentum $P_0 = mV/\sqrt{1 - (V/c)^2}$], showing that they increase both as the interaction length increases and as the electron velocity decreases, as a consequence of the properties of γ discussed in Fig. 3. However, the laterally wider and closer electron (second row) displays larger lateral momentum gain, since mirror-symmetry breaking is more pronounced close to the film [see Fig. 3(b)], and it has smaller momentum uncertainty. To quantify the efficiency of the lateral momentum transfer, in Fig. 4(c) we plot the

peak factor $\langle P_y \rangle / \sqrt{\langle P_y^2 \rangle - \langle P_y \rangle^2}$ showing that the laterally wider and closer electron (second row) experiences a lateral momentum transfer two order of magnitudes more efficient than the tightly confined and distant electron (first row). This is in agreement with the above general observation that the lateral smearing of the electron wave function dominates the mirror-symmetry breaking of its reduced density matrix. Remarkably, the lateral momentum transfer efficiency is globally larger at larger electron velocities.

V. CONCLUSIONS

In conclusion, we have shown that fast electrons with no handedness (i.e., carrying no orbital angular momentum)

can experience the microscopic chirality of geometrically symmetric samples owing to the combination of electron lateral quantum smearing with the spatial asymmetry of the electromagnetic interaction. Matter chirality breaks mirror symmetry of electron quantum decoherence, an effect detectable through biprism electron holography [43,44] or in a two-slit interference experiment [45,46]. This result is in agreement with the fact that the spatial coherence of inelastically scattered electrons is highly correlated with the optical properties of the sample. As a consequence, we predict that the electron lateral momentum distribution is asymmetric as well, thus yielding a net lateral momentum transfer which, in principle, can be detected through momentum-resolved energy-loss spectroscopy [47]. We stress that the lateral momentum gained by the electron upon scattering is entirely due matter chirality and that its detection is not hampered by other momentum exchange mechanisms since it is performed along the direction orthogonal to the setup mirror-symmetry plane. As a final remark, we stress that the whole effect allowing the electron to sense matter chirality is supported by a very tightly confined quantum electromagnetic field mediating electron-matter interaction, that is to say, it is a near-field effect. Therefore, in the presence of plasmonic samples or suitably designed plasmonic environments, electron-chiral-sample interaction can in principle be boosted by plasmonic resonances, thus enhancing the generally small electron lateral momentum gain. This could provide the basis for a chiral sensing technique where the role of the probe is played by fast electrons which are able to experience matter chirality, as opposed to photons, even though they are launched with no initial intrinsic handedness.

ACKNOWLEDGMENT

The author acknowledges PRIN 2017 PELM (Grant No. 2017PSCKT).

APPENDIX A: MACROSCOPIC QUANTUM ELECTRODYNAMICS IN CHIRAL MEDIA

MQED is a powerful tool providing a quantum description of the electromagnetic field in absorbing linear media [25,48] with any optical properties, encompassing spatial nonlocality and nonreciprocity [27]. We here review the MQED formalism in inhomogeneous chiral media characterized (in the frequency domain $e^{-i\omega t}$) by the classical constitutive relations

$$\begin{aligned} \mathbf{D}_\omega &= \epsilon_0 \epsilon \mathbf{E}_\omega - \frac{i}{c} \kappa \mathbf{H}_\omega, \\ \mathbf{B}_\omega &= \frac{i}{c} \kappa \mathbf{E}_\omega + \mu_0 \mu \mathbf{H}_\omega, \end{aligned} \quad (\text{A1})$$

where $\epsilon(\mathbf{r}, \omega)$ and $\mu(\mathbf{r}, \omega)$ are the relative permittivity and permeability and $\kappa(\mathbf{r}, \omega)$ is the Pasteur parameter controlling the coupling between electric and magnetic responses (i.e., the medium chirality); as required by causality, such parameters satisfy the Kramers-Kronig dispersion relations. The details of the general quantization scheme are reported in Ref. [27], and here we summarize the specific results pertaining chiral media.

The classical Green's tensor is among the basic tools of MQED and hence we briefly discuss some of its properties. The classical field produced by a current density distribution $\mathbf{J}_\omega(\mathbf{r})$ in the presence of a chiral medium is

$$\mathbf{E}_\omega(\mathbf{r}) = i\omega\mu_0 \int d^3\mathbf{r}' \mathcal{G}_\omega(\mathbf{r}, \mathbf{r}') \mathbf{J}_\omega(\mathbf{r}'), \quad (\text{A2})$$

where the Green's tensor $\mathcal{G}_\omega(\mathbf{r}, \mathbf{r}')$ is the solution to the inhomogeneous Helmholtz equation

$$\left\{ \nabla \times \frac{1}{\mu} \nabla \times -\frac{\omega^2}{c^2} \left(\epsilon - \frac{\kappa^2}{\mu} \right) + \frac{\omega}{c} \left[\left(\nabla \frac{\kappa}{\mu} \right) \times + 2 \frac{\kappa}{\mu} \nabla \times \right] \right\} \mathcal{G}_\omega(\mathbf{r}, \mathbf{r}') = \delta(\mathbf{r} - \mathbf{r}') I, \quad (\text{A3})$$

with the boundary conditions $\mathcal{G}_\omega(\mathbf{r}, \mathbf{r}') \rightarrow 0$ for $\mathbf{r}, \mathbf{r}' \rightarrow \infty$. Here we have considered the general inhomogeneous situation where ϵ , μ , and κ are position-dependent, which encompasses the case of piecewise homogeneous media. A relevant property of the Green's tensor $\mathcal{G}_\Omega(\mathbf{r}, \mathbf{r}')$ as a function of the complex variable Ω is that it is analytic along the whole upper half-plane $\text{Im } \Omega > 0$. In addition, it satisfies the Schwarz reflection principle

$$\mathcal{G}_\Omega^*(\mathbf{r}, \mathbf{r}') = \mathcal{G}_{-\Omega^*}(\mathbf{r}, \mathbf{r}') \quad (\text{A4})$$

and displays the asymptotic behavior

$$\mathcal{G}_\Omega(\mathbf{r}, \mathbf{r}') \rightarrow -\frac{c^2}{\Omega^2} \delta(\mathbf{r} - \mathbf{r}') \quad (\text{A5})$$

for $\Omega \rightarrow \infty$. By using all these properties it is simple to show that the imaginary part of the Green's tensor satisfies the important integral relation

$$\int_0^{+\infty} d\omega \omega \text{Im}[\mathcal{G}_\omega(\mathbf{r}, \mathbf{r}')] = \frac{\pi}{2} c^2 \delta(\mathbf{r} - \mathbf{r}') I. \quad (\text{A6})$$

Since chiral media are reciprocal, the Green's tensor satisfies the Onsager reciprocity relation

$$\mathcal{G}_\omega^T(\mathbf{r}, \mathbf{r}') = \mathcal{G}_\omega(\mathbf{r}', \mathbf{r}) \quad (\text{A7})$$

which arises in connection with the fluctuation-dissipation theorem.

Medium absorption forbids regarding radiation as an isolated system and hence, as suggested by the fluctuation-dissipation theorem, a noise current $\mathbf{j}_\omega^N(\mathbf{r})$ is introduced to account for the medium degrees of freedom. Moreover, the noise current encodes the full radiation-medium state since its radiated field is provided by $\mathbf{E}_\omega(\mathbf{r}) = i\omega\mu_0 \int d^3\mathbf{r}' \mathcal{G}_\omega(\mathbf{r}, \mathbf{r}') \mathbf{j}_\omega^N(\mathbf{r}')$ [see Eq. (A2)]. Quantization is performed by requiring that the electric and magnetic induction field operators satisfy the standard vacuum quantum electrodynamic commutation relations, and this leads to a radiation-medium description in terms of boson polaritonic excitations. Due to magnetoelectric coupling, both electric (e) and magnetic (m) contributions of the noise currents are involved, and hence two field operators, $\hat{\mathbf{f}}_{\omega e}(\mathbf{r}) = \hat{f}_{\omega ej}(\mathbf{r}) \mathbf{e}_j$ and $\hat{\mathbf{f}}_{\omega m}(\mathbf{r}) = \hat{f}_{\omega mj}(\mathbf{r}) \mathbf{e}_j$, are introduced in the Schrödinger picture whose components satisfy the commutation relations

$$\begin{aligned} & [\hat{f}_{\omega\lambda j}(\mathbf{r}), \hat{f}_{\omega'\lambda'j'}(\mathbf{r}')] = 0, \\ & [\hat{f}_{\omega\lambda j}(\mathbf{r}), \hat{f}_{\omega'\lambda'j'}^\dagger(\mathbf{r}')] = \delta(\omega - \omega') \delta_{\lambda\lambda'} \delta_{jj'} \delta(\mathbf{r} - \mathbf{r}'), \end{aligned} \quad (\text{A8})$$

so that $\hat{f}_{\omega\lambda j}^\dagger(\mathbf{r})$ is the creation operator of the j component of a polaritonic excitation of frequency ω and type $\lambda = e, m$ at position \mathbf{r} . The electromagnetic Hamiltonian is

$$\hat{H}_{\text{em}} = \int_0^\infty d\omega \hbar \omega \sum_\lambda \int d^3\mathbf{r} \hat{\mathbf{f}}_{\omega\lambda}^\dagger(\mathbf{r}) \cdot \hat{\mathbf{f}}_{\omega\lambda}(\mathbf{r}) \quad (\text{A9})$$

since it predicts the correct time evolution of the annihilation operators

$$e^{(i/\hbar)\hat{H}_{\text{em}}t} \hat{\mathbf{f}}_{\omega\lambda} e^{-(i/\hbar)\hat{H}_{\text{em}}t} = \hat{\mathbf{f}}_{\omega\lambda} e^{-i\omega t}. \quad (\text{A10})$$

The electric field operator $\hat{\mathbf{E}} = \int_0^{+\infty} d\omega (\hat{\mathbf{E}}_\omega + \hat{\mathbf{E}}_\omega^\dagger)$ has positive frequency part

$$\hat{\mathbf{E}}_\omega(\mathbf{r}) = \sum_\lambda \int d^3\mathbf{r}' \mathcal{G}_{\omega\lambda}(\mathbf{r}, \mathbf{r}') \hat{\mathbf{f}}_{\omega\lambda}(\mathbf{r}'), \quad (\text{A11})$$

where the tensors $\mathcal{G}_{\omega e}$ and $\mathcal{G}_{\omega m}$ are obtained from the Green's tensor \mathcal{G}_ω via

$$\begin{aligned} \begin{pmatrix} \mathcal{G}_{\omega e} \\ \mathcal{G}_{\omega m} \end{pmatrix}_{(\mathbf{r}, \mathbf{r}')} &= -i\omega\mu_0 \sqrt{\frac{\hbar}{\pi}} \begin{pmatrix} U_{ee} & U_{em} \\ U_{me} & U_{mm} \end{pmatrix}_{(\mathbf{r})} \\ &\times \begin{pmatrix} i\omega\mathcal{G}_\omega \\ \mathcal{G}_\omega \times \vec{\nabla} \end{pmatrix}_{(\mathbf{r}, \mathbf{r}')}, \end{aligned} \quad (\text{A12})$$

with the matrix $U_{\lambda\lambda'}$ satisfying the equation

$$\begin{pmatrix} U_{ee} & U_{em} \\ U_{me} & U_{mm} \end{pmatrix}^{*T} \begin{pmatrix} U_{ee} & U_{em} \\ U_{me} & U_{mm} \end{pmatrix} = \begin{pmatrix} \varepsilon_0 \text{Im}\left(\varepsilon - \frac{\kappa^2}{\mu}\right) & i\sqrt{\frac{\varepsilon_0}{\mu_0}} \text{Im}\left(\frac{\kappa}{\mu}\right) \\ -i\sqrt{\frac{\varepsilon_0}{\mu_0}} \text{Im}\left(\frac{\kappa}{\mu}\right) & -\frac{1}{\mu_0} \text{Im}\left(\frac{1}{\mu}\right) \end{pmatrix}. \quad (\text{A13})$$

It is worth noting that the tensors $\mathcal{G}_{\omega e}$ and $\mathcal{G}_{\omega m}$ satisfy the identity

$$\sum_\lambda \int d^3\mathbf{s} \mathcal{G}_{\omega\lambda}(\mathbf{r}, \mathbf{s}) \mathcal{G}_{\omega\lambda}^{*T}(\mathbf{r}', \mathbf{s}) = \frac{\hbar\omega^2}{\pi\varepsilon_0 c^2} \text{Im}[\mathcal{G}_\omega(\mathbf{r}, \mathbf{r}')], \quad (\text{A14})$$

which is very useful since, among other things, when combined with Eqs. (A8) and (A11), it yields the relation

$$\begin{aligned} & [\mathbf{F} \cdot \hat{\mathbf{E}}_\omega(\mathbf{r}), \mathbf{F}' \cdot \hat{\mathbf{E}}_\omega^\dagger(\mathbf{r}')] \\ &= \delta(\omega - \omega') \frac{\hbar\omega^2}{\pi\varepsilon_0 c^2} \mathbf{F} \cdot \text{Im}[\mathcal{G}_\omega(\mathbf{r}, \mathbf{r}')] \mathbf{F}' \end{aligned} \quad (\text{A15})$$

where \mathbf{F} and \mathbf{F}' are two vectors. Equation (A15) provides the commutator of electric field components at different points and different frequencies and highlights the role played by the imaginary part of the Green's tensor.

In order to deal with the electron-radiation coupling, the vector and scalar potentials, $\hat{\mathbf{A}} = \int_0^{+\infty} d\omega (\hat{\mathbf{A}}_\omega + \hat{\mathbf{A}}_\omega^\dagger)$ and $\hat{\phi} = \int_0^{+\infty} d\omega (\hat{\phi}_\omega + \hat{\phi}_\omega^\dagger)$, are required. Their positive-frequency parts are defined by the relation $\hat{\mathbf{E}}_\omega = i\omega\hat{\mathbf{A}}_\omega - \nabla\hat{\phi}_\omega$ so that, after choosing the Coulomb gauge $\nabla \cdot \hat{\mathbf{A}}_\omega = 0$, the terms $i\omega\hat{\mathbf{A}}_\omega$ and $-\nabla\hat{\phi}_\omega$ can be identified with the transverse and longitudinal parts of the field $\hat{\mathbf{E}}_\omega$ so that

$$\begin{aligned} \hat{\mathbf{A}}_\omega(\mathbf{r}) &= \frac{1}{i\omega} \int d^3\mathbf{r}' \left[\frac{1}{(2\pi)^3} \int d^3\mathbf{k} e^{i\mathbf{k} \cdot (\mathbf{r} - \mathbf{r}')} \left(I - \frac{\mathbf{k}\mathbf{k}}{k^2} \right) \right] \\ &\times \hat{\mathbf{E}}_\omega(\mathbf{r}'), \\ \hat{\phi}_\omega(\mathbf{r}) &= \int d^3\mathbf{r}' \left[\frac{1}{(2\pi)^3} \int d^3\mathbf{k} e^{i\mathbf{k} \cdot (\mathbf{r} - \mathbf{r}')} \frac{i\mathbf{k}}{k^2} \right] \cdot \hat{\mathbf{E}}_\omega(\mathbf{r}'). \end{aligned} \quad (\text{A16})$$

We highlight that the choice of the Coulomb gauge is not incompatible with a possible spatial inhomogeneity of the medium (responsible for $\nabla \cdot \hat{\mathbf{E}}_\omega \neq 0$) since we are describing the electromagnetic field by means of both the vector and scalar potentials. This is made manifest by rewriting

Eqs. (A16) as

$$\hat{\mathbf{A}}_\omega(\mathbf{r}) = \frac{1}{i\omega} \left[\hat{\mathbf{E}}_\omega(\mathbf{r}) + \nabla \int d^3\mathbf{r}' \frac{\nabla' \cdot \hat{\mathbf{E}}_\omega(\mathbf{r}')}{4\pi |\mathbf{r} - \mathbf{r}'|} \right], \quad (\text{A17})$$

$$\hat{\phi}_\omega(\mathbf{r}) = \int d^3\mathbf{r}' \frac{\nabla' \cdot \hat{\mathbf{E}}_\omega(\mathbf{r}')}{4\pi |\mathbf{r} - \mathbf{r}'|},$$

where we have used the Fourier integral representation of the Coulomb potential

$$\frac{1}{4\pi r} = \frac{1}{(2\pi)^3} \int d^3\mathbf{k} \frac{e^{i\mathbf{k}\cdot\mathbf{r}}}{k^2}. \quad (\text{A18})$$

APPENDIX B: INTERACTION HAMILTONIAN AND S-OPERATOR

The minimal coupling Hamiltonian describing a relativistic electron interacting with a chiral medium is

$$\hat{H} = c\sqrt{m^2c^2 + [\hat{\mathbf{P}} + e\hat{\mathbf{A}}(\hat{\mathbf{R}})]^2} - e\hat{\phi}(\hat{\mathbf{R}}) + \hat{H}_{\text{em}}, \quad (\text{B1})$$

where m and $-e < 0$ are the electron rest mass and charge, $\hat{\mathbf{R}}$ and $\hat{\mathbf{P}}$ are the electron position and momentum operators ($[\hat{\mathbf{R}}, \hat{\mathbf{P}}] = i\hbar I$), $\hat{\mathbf{A}}$ and $\hat{\phi}$ are the vector and scalar potentials defined in Appendix A, and \hat{H}_{em} is the electromagnetic Hamiltonian defined in Eq. (A9). Since $\hat{\mathbf{A}} \cdot \hat{\mathbf{P}} - \hat{\mathbf{P}} \cdot \hat{\mathbf{A}} = i\hbar\nabla \cdot \hat{\mathbf{A}}$, the transversality of the vector potential in the Coulomb gauge implies that $(\hat{\mathbf{P}} + e\hat{\mathbf{A}})^2 = \hat{P}^2 + 2e\hat{\mathbf{A}} \cdot \hat{\mathbf{P}} + e\hat{A}^2$ and hence, by exploiting the weakness of the electron-radiation coupling, the term $e^2\hat{A}^2$ can be neglected while the square root can be expanded up to the first order in the term $2e\hat{\mathbf{A}} \cdot \hat{\mathbf{P}}$, thus obtaining

$$\hat{H} = c\sqrt{m^2c^2 + \hat{P}^2} + e\frac{c}{\sqrt{m^2c^2 + \hat{P}^2}} \hat{\mathbf{A}}(\hat{\mathbf{R}}) \cdot \hat{\mathbf{P}} - e\hat{\phi}(\hat{\mathbf{R}}) + \hat{H}_{\text{em}}. \quad (\text{B2})$$

To further simplify the Hamiltonian, we now perform the standard paraxial approximation, which is adequate for dealing with highly collimated electron beams routinely used in transmission electron microscopes. Accordingly, we consider electron states whose momentum distribution is strongly localized around a central momentum \mathbf{P}_0 ($|\hat{\mathbf{P}} - \mathbf{P}_0| \ll P_0$) so that, by linearizing the first term of Eq. (B2) around \mathbf{P}_0 and evaluating the second term at \mathbf{P}_0 , after neglecting an irrelevant constant contribution, we get

$$\hat{H} = \underbrace{\mathbf{V} \cdot \hat{\mathbf{P}} + \hat{H}_{\text{em}}}_{\hat{H}_0} + e \underbrace{\left[\mathbf{V} \cdot \hat{\mathbf{A}}(\hat{\mathbf{R}}) - \hat{\phi}(\hat{\mathbf{R}}) \right]}_{\hat{H}_{\text{int}}} \quad (\text{B3})$$

where $\mathbf{V} = c\mathbf{P}_0/\sqrt{m^2c^2 + P_0^2}$. Due to the relation

$$e^{(i/\hbar)(\mathbf{V} \cdot \hat{\mathbf{P}})t} \hat{\mathbf{R}} e^{-(i/\hbar)(\mathbf{V} \cdot \hat{\mathbf{P}})t} = \hat{\mathbf{R}} + \mathbf{V}t, \quad (\text{B4})$$

the vector \mathbf{V} can be interpreted as the free electron velocity which is independent of momentum due to paraxial approximation. As highlighted by the curly brackets, the Hamiltonian has a main term \hat{H}_0 accounting for the bare electron-radiation system and a term \hat{H}_{int} describing their coupling. By using Eq. (A9) and Eqs. (A17) we get

$$\begin{aligned} \hat{H}_0 &= \mathbf{V} \cdot \hat{\mathbf{P}} + \int_0^\infty d\omega \hbar \omega \sum_\lambda \int d^3\mathbf{r} \hat{\mathbf{f}}_{\omega\lambda}^\dagger(\mathbf{r}) \cdot \hat{\mathbf{f}}_{\omega\lambda}(\mathbf{r}), \\ \hat{H}_{\text{int}} &= \int_0^{+\infty} d\omega \frac{e}{i\omega} \int d^3\mathbf{r} \left[\mathbf{Q}_\omega(\hat{\mathbf{R}}, \mathbf{r}) \cdot \hat{\mathbf{E}}_\omega(\mathbf{r}) \right. \\ &\quad \left. - \mathbf{Q}_\omega^*(\hat{\mathbf{R}}, \mathbf{r}) \cdot \hat{\mathbf{E}}_\omega^\dagger(\mathbf{r}) \right], \end{aligned} \quad (\text{B5})$$

where

$$\mathbf{Q}_\omega(\mathbf{R}, \mathbf{r}) = \delta(\mathbf{R} - \mathbf{r}) \mathbf{V} + (\mathbf{V} \cdot \nabla_{\mathbf{R}} - i\omega) \frac{1}{4\pi |\mathbf{R} - \mathbf{r}|} \nabla_{\mathbf{r}}. \quad (\text{B6})$$

The delta function contribution of \mathbf{Q}_ω provides the direct interaction between the electron and the radiation electric field whereas the other contribution accounts for the coupling of the electron with the Coulomb field produced by the medium inhomogeneity.

Let us now consider a typical scattering situation where a free electron in the distant past is made to interact with the chiral medium and is subsequently collected by a detector in the far future. The time evolution of an initial electron-radiation state $|\Psi_i\rangle = |\Psi(-\infty)\rangle$, in the interaction picture, is provided by $|\Psi(t)\rangle = \hat{U}(t)|\Psi_i\rangle$ where the time evolution operator $\hat{U}(t)$ is the solution of the equation

$$i\hbar \frac{d\hat{U}}{dt} = \left(e^{(i/\hbar)\hat{H}_0 t} \hat{H}_{\text{int}} e^{-(i/\hbar)\hat{H}_0 t} \right) \hat{U} \quad (\text{B7})$$

with initial value $\hat{U}(-\infty) = 1$. The dynamics of fast electrons interacting with nonmagnetoelectric media has been investigated to some extent [29,31,37] and we extend those results here to chiral media. We start by using Eqs. (A10) and Eqs. (B4) to cast Eq. (B7) as

$$\frac{d\hat{U}}{dt} = \left\{ \int_0^{+\infty} d\omega \int d^3 \mathbf{r} \frac{e}{\hbar\omega} \left[-e^{-i\omega t} \mathbf{Q}_\omega(\hat{\mathbf{R}} + \mathbf{V}t, \mathbf{r}) \cdot \hat{\mathbf{E}}_\omega(\mathbf{r}) + e^{i\omega t} \mathbf{Q}_\omega^*(\hat{\mathbf{R}} + \mathbf{V}t, \mathbf{r}) \cdot \hat{\mathbf{E}}_\omega^\dagger(\mathbf{r}) \right] \right\} \hat{U}, \quad (\text{B8})$$

which we solve by means of the trial solution

$$\hat{U} = e^{i\hat{W}}, \quad (\text{B9})$$

where

$$\hat{W} = \Xi(\hat{\mathbf{R}}, t) + \int_0^{+\infty} d\omega \int d^3 \mathbf{r} \left[\mathbf{N}_\omega(\hat{\mathbf{R}}, \mathbf{r}, t) \cdot \hat{\mathbf{E}}_\omega(\mathbf{r}) + \mathbf{N}_\omega^*(\hat{\mathbf{R}}, \mathbf{r}, t) \cdot \hat{\mathbf{E}}_\omega^\dagger(\mathbf{r}) \right], \quad (\text{B10})$$

and the unknown function Ξ and vector \mathbf{N}_ω are such that $\Xi(\hat{\mathbf{R}}, -\infty) = 0$ and $\mathbf{N}_\omega(\hat{\mathbf{R}}, \mathbf{r}, -\infty) = 0$, as required by the initial value of \hat{U} . In order to substitute Eq. (B9) into Eq. (B8), we use Sneddon's formula for the derivative of the exponential of an operator [49],

$$\frac{d}{dt} e^{i\hat{W}} = i \int_0^1 d\varphi e^{i\varphi \hat{W}} \frac{d\hat{W}}{dt} e^{i(1-\varphi)\hat{W}}, \quad (\text{B11})$$

whose evaluation requires the analysis of the commutator of \hat{W} and $d\hat{W}/dt$. From Eq. (A15), we easily get

$$\left[\hat{W}, \frac{d\hat{W}}{dt} \right] = \frac{2i\hbar}{\pi\varepsilon_0 c^2} \int_0^{+\infty} d\omega \omega^2 \int d^3 \mathbf{r} \int d^3 \mathbf{r}' \text{Im} \left\{ \mathbf{N}_\omega(\hat{\mathbf{R}}, \mathbf{r}, t) \cdot \text{Im} [\mathcal{G}_\omega(\mathbf{r}, \mathbf{r}')] \frac{\partial \mathbf{N}_\omega^*(\hat{\mathbf{R}}, \mathbf{r}', t)}{\partial t} \right\} \quad (\text{B12})$$

whose independence of the polaritonic operators $\hat{\mathbf{f}}_{\omega\lambda}, \hat{\mathbf{f}}_{\omega\lambda}^\dagger$ implies that it commutes with both \hat{W} and $d\hat{W}/dt$. As a consequence, the relation $[e^{i\xi\hat{W}}, (d\hat{W}/dt)] = [\hat{W}, (d\hat{W}/dt)] i\xi e^{i\xi\hat{W}}$ allows Eq. (B11) to be written as

$$\frac{d}{dt} e^{i\hat{W}} = \left(-\frac{1}{2} \left[\hat{W}, \frac{d\hat{W}}{dt} \right] + i \frac{d\hat{W}}{dt} \right) e^{i\hat{W}} \quad (\text{B13})$$

which, when compared with Eq. (B8), states that $e^{i\hat{W}}$ is the evolution operator if

$$\frac{\partial \mathbf{N}_\omega}{\partial t} = \frac{ie}{\hbar\omega} e^{-i\omega t} \mathbf{Q}_\omega(\hat{\mathbf{R}} + \mathbf{V}t, \mathbf{r}), \quad (\text{B14a})$$

$$\frac{\partial \Xi}{\partial t} = \frac{1}{2i} \left[\hat{W}, \frac{d\hat{W}}{dt} \right]. \quad (\text{B14b})$$

Noting that Eq. (B6) yields

$$e^{-i\omega t} \mathbf{Q}_\omega(\hat{\mathbf{R}} + \mathbf{V}t, \mathbf{r}) = e^{-i\omega t} \delta(\hat{\mathbf{R}} - \mathbf{r} + \mathbf{V}t) \mathbf{V} + \frac{d}{dt} \left[\frac{e^{-i\omega t}}{4\pi|\hat{\mathbf{R}} + \mathbf{V}t - \mathbf{r}|} \nabla_{\mathbf{r}} \right], \quad (\text{B14c})$$

the integration of Eq. (B14a) is straightforward and we get

$$\mathbf{N}_\omega(\hat{\mathbf{R}}, \mathbf{r}, t) = \frac{ie}{\hbar\omega} \left[e^{i(\omega/V)(\hat{R}_v - r_v)} \delta(\hat{\mathbf{R}}_t - \mathbf{r}_t) \theta(\hat{R}_v - r_v + Vt) \mathbf{u}_v + \frac{e^{-i\omega t}}{4\pi|\hat{\mathbf{R}} + \mathbf{V}t - \mathbf{r}|} \nabla_{\mathbf{r}} \right], \quad (\text{B15})$$

where $\theta(\xi)$ is the unit step function, $\mathbf{u}_v = \mathbf{V}/V$ is the electron velocity unit vector, and we have introduced the decomposition $\mathbf{F} = \mathbf{F}_t + \mathbf{F}_v$ of a vector \mathbf{F} into its parts transverse (t) and parallel (v) to \mathbf{V} , namely,

$$\begin{aligned} \mathbf{F}_t &= \mathbf{F} - (\mathbf{u}_v \cdot \mathbf{F}) \mathbf{u}_v, \\ \mathbf{F}_v &= (\mathbf{u}_v \cdot \mathbf{F}) \mathbf{u}_v \equiv F_v \mathbf{u}_v. \end{aligned} \quad (\text{B16})$$

Equation (B14b) can also be integrated by using Eqs. (B12) and (B16) and, after some tedious but straightforward algebra, we get

$$\begin{aligned} \Xi(\hat{\mathbf{R}}, t) = & \frac{4\alpha}{c} \text{Im} \int_0^{+\infty} d\omega \int_{-\infty}^{\hat{R}_v + Vt} dr_v \int_{-\infty}^{r_v} dr'_v e^{i(\omega/V)(r_v - r'_v)} \text{Im} \left[\mathbf{u}_v \cdot \mathcal{G}_\omega(\hat{\mathbf{R}}_t + r_v \mathbf{u}_v, \hat{\mathbf{R}}_t + r'_v \mathbf{u}_v) \mathbf{u}_v \right] \\ & + \frac{\alpha}{\pi c} \text{Im} \int_0^{+\infty} d\omega \int d^3 \mathbf{r} \int_{-\infty}^{\hat{R}_v + Vt} dr'_v \frac{e^{i(\omega/V)(\hat{R}_v + Vt - r'_v)}}{|\hat{\mathbf{R}} + \mathbf{V}t - \mathbf{r}|} \nabla_{\mathbf{r}} \cdot \text{Im} \left[\mathcal{G}_\omega(\mathbf{r}, \hat{\mathbf{R}}_t + r'_v \mathbf{u}_v) \right] \mathbf{u}_v \\ & + \frac{\alpha}{4\pi^2 c} \int_0^{+\infty} d\omega \omega \int d^3 \mathbf{r} \int d^3 \mathbf{r}' \int_{-\infty}^t d\tau \frac{\nabla_{\mathbf{r}} \cdot \text{Im} [\mathcal{G}_\omega(\mathbf{r}, \mathbf{r}')] \overleftarrow{\nabla}_{\mathbf{r}'}}{|\hat{\mathbf{R}} + \mathbf{V}\tau - \mathbf{r}| |\hat{\mathbf{R}} + \mathbf{V}\tau - \mathbf{r}'|}, \end{aligned} \quad (\text{B17})$$

where

$$\alpha = \frac{e^2}{4\pi \epsilon_0 \hbar c} \cong \frac{1}{137} \quad (\text{B18})$$

is the fine structure constant. By using the integral relation of Eq. (A6) it is simple to prove that the last contribution in Eq. (B18) can be written as

$$\frac{\alpha}{4\pi^2 c} \int_0^{+\infty} d\omega \omega \int d^3 \mathbf{r} \int d^3 \mathbf{r}' \int_{-\infty}^t d\tau \frac{\nabla_{\mathbf{r}} \cdot \text{Im} [\mathcal{G}_\omega(\mathbf{r}, \mathbf{r}')] \overleftarrow{\nabla}_{\mathbf{r}'}}{|\hat{\mathbf{R}} + \mathbf{V}\tau - \mathbf{r}| |\hat{\mathbf{R}} + \mathbf{V}\tau - \mathbf{r}'|} = \frac{\alpha c}{2} \int_{-\infty}^t d\tau \int_0^\infty dr \frac{1}{r^2} \quad (\text{B19})$$

which, although infinite, will be omitted since it provides an unobservable phase factor (being independent of $\hat{\mathbf{R}}$). By inserting Eqs. (B16) and (B18) into Eq. (B10), we get the full time evolution operator $\hat{U} = e^{i\hat{W}}$, given by

$$\hat{U} = \exp \left[i\Xi(\hat{\mathbf{R}}, t) \right] \exp \left\{ i \int_0^{+\infty} d\omega \int d^3 \mathbf{r} \left[\mathbf{N}_\omega(\hat{\mathbf{R}}, \mathbf{r}, t) \cdot \hat{\mathbf{E}}_\omega(\mathbf{r}) + \mathbf{N}_\omega^*(\hat{\mathbf{R}}, \mathbf{r}, t) \cdot \hat{\mathbf{E}}_\omega^\dagger(\mathbf{r}) \right] \right\}, \quad (\text{B20})$$

and two observations are in order. First, if the medium inhomogeneity is weak, all the terms containing the gradient operator $\nabla_{\mathbf{r}}$ can be neglected since it operates on the electric field (or the Green's tensor) whose divergence is vanishingly small together with the volume charge density. In this circumstance the expression for \hat{U} coincides with that deduced in the literature for nonmagnetoelectric media [apart from the expression for the electric field in Eq. (A11) which is different due to the presence of both electric and magnetic polaritonic excitations]. Second, in the limiting case $t \rightarrow +\infty$ with which we are mainly concerned here, the terms displaying the denominator $|\mathbf{R} + \mathbf{V}\tau - \mathbf{r}|$ in Eqs. (B16) and (B18) vanish since they explicitly contain the Coulomb potential evaluated at the infinitely far position of the electron, and accordingly the S -operator $\hat{S} = \hat{U}(+\infty)$ turns out to be

$$\hat{S} = e^{i\Phi(\hat{\mathbf{R}})} e^{\hat{a}^\dagger(\hat{\mathbf{R}}) - \hat{a}(\hat{\mathbf{R}})} \quad (\text{B21})$$

where, after relabeling $r_v \rightarrow q$ and $r'_v \rightarrow q'$, we have introduced the phase factor Φ and the operator \hat{a} which, for a vector \mathbf{F} , are given by

$$\begin{aligned} \Phi(\mathbf{F}) &= \frac{4\alpha}{c} \int_0^{+\infty} d\omega \int_{-\infty}^{+\infty} dq \int_{-\infty}^q dq' \sin \left[\frac{\omega}{V}(q - q') \right] \text{Im} \left[\mathbf{u}_v \cdot \mathcal{G}_\omega(\mathbf{F}_t + q\mathbf{u}_v, \mathbf{F}_t + q'\mathbf{u}_v) \mathbf{u}_v \right], \\ \hat{a}(\mathbf{F}) &= \int_0^{+\infty} d\omega \frac{e}{\hbar\omega} \int_{-\infty}^{+\infty} dq e^{i(\omega/V)(F_v - q)} \mathbf{u}_v \cdot \hat{\mathbf{E}}_\omega(\mathbf{F}_t + q\mathbf{u}_v). \end{aligned} \quad (\text{B22})$$

Note that the phase factor $\Phi(\mathbf{F}) = \Phi(\mathbf{F}_t)$ only depends on the transverse part \mathbf{F}_t of the vector \mathbf{F} . We stress that the S -operator obtained in Eq. (B22) coincides with the one discussed in the literature for nonmagnetoelectric media, and we have extended its validity here to chiral media in full generality.

The commutator of $\hat{a}(\hat{\mathbf{R}})$ and $\hat{a}^\dagger(\hat{\mathbf{R}})$ is easily evaluated by means of Eq. (A15) and turns out to be

$$\left[\hat{a}(\hat{\mathbf{R}}), \hat{a}^\dagger(\hat{\mathbf{R}}) \right] = \Delta(\hat{\mathbf{R}}, \hat{\mathbf{R}}), \quad (\text{B23})$$

where we have introduced the function of two vectors \mathbf{F} and \mathbf{F}' ,

$$\begin{aligned} \Delta(\mathbf{F}, \mathbf{F}') &= \frac{4\alpha}{c} \int_0^\infty d\omega e^{-i(\omega/V)(F_v - F'_v)} \\ &\times \int_{-\infty}^{+\infty} dq \int_{-\infty}^{+\infty} dq' e^{i(\omega/V)(q - q')} \\ &\times \text{Im} [\mathbf{u}_v \cdot \mathcal{G}_\omega (\mathbf{F}_t + q\mathbf{u}_v, \mathbf{F}'_t + q'\mathbf{u}_v) \mathbf{u}_v], \end{aligned} \quad (\text{B24})$$

which plays a fundamental role in our analysis. Note that the Onsager reciprocity of the Green's tensor [see Eq. (A7)] implies that

$$\Delta(\mathbf{F}', \mathbf{F}) = \Delta^*(\mathbf{F}, \mathbf{F}') \quad (\text{B25})$$

and consequently $\Delta(\mathbf{F}, \mathbf{F})$ is a real number and $\Delta(\hat{\mathbf{R}}, \hat{\mathbf{R}})$ is a hermitian operator in agreement with the fact that, from Eq. (B24), it is the commutator of two hermitian conjugated operators. Note also that the relation

$$\Delta(\mathbf{F}, \mathbf{F}') = \Delta(\mathbf{F}_t + (F_v - F'_v) \mathbf{u}_v, \mathbf{F}'_t) \quad (\text{B26})$$

holds, so that $\Delta(\mathbf{F}, \mathbf{F}) = \Delta(\mathbf{F}_t, \mathbf{F}'_t)$ only depends on \mathbf{F}_t . Since both $\hat{a}(\hat{\mathbf{R}})$ and $\hat{a}^\dagger(\hat{\mathbf{R}})$ evidently commute with their commutator, we can resort to the Baker-Campbell-Hausdorff identity $e^{\hat{X} + \hat{Y}} = e^{-(1/2)[\hat{X}, \hat{Y}]} e^{\hat{X}} e^{\hat{Y}}$ to cast Eq. (B22) in the form

$$\hat{S} = e^{i\Phi(\hat{\mathbf{R}}_t)} e^{-(1/2)\Delta(\hat{\mathbf{R}}_t, \hat{\mathbf{R}}_t)} e^{\hat{a}^\dagger(\hat{\mathbf{R}})} e^{-\hat{a}(\hat{\mathbf{R}})} \quad (\text{B27})$$

where we have made explicit the dependence of Φ and Δ (with equal arguments) on the transverse component $\hat{\mathbf{R}}_t$ of the position operator.

APPENDIX C: ELECTRON REDUCED DENSITY MATRIX

The S -operator obtained in the above section provides the full time evolution of the initial electron-radiation state $|\Psi_i\rangle$ toward the final state $|\Psi\rangle = \hat{S}|\Psi_i\rangle$. Since radiation is not excited at first, the initial state we choose is

$$|\Psi_i\rangle = |\psi_i, 0\rangle \equiv |\psi_i\rangle \otimes |0\rangle \quad (\text{C1})$$

where $|\psi_i\rangle$ is a free electron state of energy E_i [11], that is,

$$\mathbf{V} \cdot \hat{\mathbf{P}} |\psi_i\rangle = E_i |\psi_i\rangle, \quad (\text{C2})$$

and $|0\rangle$ is the vacuum radiation state defined by $\hat{f}_{\omega\lambda j}(\mathbf{r})|0\rangle = 0$. Accordingly $|\Psi_i\rangle$ is an eigenstate of \hat{H}_0

with eigenvalue E_i . After applying the S -operator of Eq. (B28) to this initial state and, using the second part of Eqs. (B23) and (A11), we get

$$\begin{aligned} |\Psi\rangle &= e^{i\Phi(\hat{\mathbf{R}}_t)} e^{-(1/2)\Delta(\hat{\mathbf{R}}_t, \hat{\mathbf{R}}_t)} \sum_{n=0}^{\infty} \frac{1}{n!} \left[\int d\xi T(\hat{\mathbf{R}}, \xi) \hat{f}^\dagger(\xi) \right]^n \\ &\times |\psi_i, 0\rangle, \end{aligned} \quad (\text{C3})$$

where the exponential of $\hat{a}^\dagger(\hat{\mathbf{R}})$ has been expanded, we have introduced the compact index $\xi = (\omega, \lambda, j, \mathbf{r})$ to label the elementary polaritonic excitation and, for notational convenience, we have set

$$\begin{aligned} \hat{f}(\xi) &= \hat{f}_{\omega\lambda j}(\mathbf{r}), \\ \int d\xi &= \int d\omega \sum_{\lambda j} \int d^3\mathbf{r}, \\ T(\hat{\mathbf{R}}, \xi) &= \frac{e}{\hbar\omega} \int_{-\infty}^{+\infty} dq e^{-i(\omega/V)(\hat{R}_v - q)} \mathbf{u}_v \\ &\cdot \mathcal{G}_{\omega\lambda}^*(\hat{\mathbf{R}}_t + q\mathbf{u}_v, \mathbf{r}) \mathbf{e}_j. \end{aligned} \quad (\text{C4})$$

In order to analyze the final state $|\Psi\rangle$, it is convenient to use the representation provided by the states

$$|\mathbf{R}, \xi_1 \dots \xi_n\rangle = |\mathbf{R}\rangle \otimes \left[\frac{1}{\sqrt{n!}} \hat{f}^\dagger(\xi_1) \dots \hat{f}^\dagger(\xi_n) |0\rangle \right] \quad (\text{C5})$$

where $|\mathbf{R}\rangle$ is the eigenvector of the electron position operator $\hat{\mathbf{R}}$ (i.e., $\hat{\mathbf{R}}|\mathbf{R}\rangle = \mathbf{R}|\mathbf{R}\rangle$). The state $|\mathbf{R}, \xi_1 \dots \xi_n\rangle$ corresponds to the electron at the position \mathbf{R} and the radiation with n quanta distributed on the n polaritonic excitations $\xi_1 \dots \xi_n$. These states are an orthonormal basis of the tensor product of the electron Hilbert space and the radiation Fock space due to the relations

$$\begin{aligned} &\langle \mathbf{R}, \xi_1 \dots \xi_n | \mathbf{R}', \xi'_1 \dots \xi'_{n'} \rangle \\ &= \delta(\mathbf{R} - \mathbf{R}') \frac{\delta_{n,n'}}{n!} \sum_{\pi \in S_n} [\delta(\xi_1 - \xi'_{\pi(1)}) \dots \delta(\xi_n - \xi'_{\pi(n)})], \\ &\int d^3\mathbf{R} \sum_{n=0}^{\infty} \int d\xi_1 \dots d\xi_n |\mathbf{R}, \xi_1 \dots \xi_n\rangle \langle \mathbf{R}, \xi_1 \dots \xi_m| = I, \end{aligned} \quad (\text{C6})$$

where the sum in the first equation spans the $n!$ permutation π of the symmetric group S_n and

$$\delta(\xi - \xi') = \delta(\omega - \omega') \delta_{\lambda\lambda'} \delta_{jj'} \delta(\mathbf{r} - \mathbf{r}'). \quad (\text{C7})$$

Accordingly, the state $|\Psi\rangle$ of Eq. (C3) can be written as

$$\begin{aligned} |\Psi\rangle &= \int d^3\mathbf{R} \sum_{n=0}^{\infty} \int d\xi_1 \dots d\xi_n |\mathbf{R}, \xi_1 \dots \xi_n\rangle \\ &\times \langle \mathbf{R}, \xi_1 \dots \xi_n | \Psi \rangle \end{aligned} \quad (\text{C8})$$

where

$$\langle \mathbf{R}, \xi_1 \dots \xi_n | \Psi \rangle = \psi_i(\mathbf{R}) e^{i\Phi(\mathbf{R}_t)} e^{-(1/2)\Delta(\mathbf{R}_t, \mathbf{R}_t)} \times \frac{1}{\sqrt{n!}} T(\mathbf{R}, \xi_1) \dots T(\mathbf{R}, \xi_n), \quad (\text{C9})$$

in which $\psi_i(\mathbf{R}) = \langle \mathbf{R} | \psi_i \rangle$ is the initial electron wave function. Equation (C8) clearly reveals the entanglement between electron and radiation created by their interaction produced by the chiral medium. In the present work we are mainly interested in spatial effects produced by the chiral medium on the electron state, regardless of the radiation state. Accordingly, due to the entanglement, it is necessary to describe the electron in terms of its reduced density operator $\hat{\rho}_e$ obtained by taking the partial trace of the density operator $\hat{\rho} = |\Psi\rangle\langle\Psi|$ over the radiation states. In the position representation which is here the most convenient one, we have

$$\hat{\rho}_e = \int d^3\mathbf{R} \int d^3\mathbf{R}' \rho_e(\mathbf{R}, \mathbf{R}') |\mathbf{R}\rangle\langle\mathbf{R}'| \quad (\text{C10})$$

where the reduced density matrix is

$$\rho_e(\mathbf{R}, \mathbf{R}') = \sum_{n=0}^{\infty} \int d\xi_1 \dots d\xi_n \langle \mathbf{R}, \xi_1 \dots \xi_n | \Psi \rangle \times \langle \Psi | \mathbf{R}', \xi_1 \dots \xi_n \rangle. \quad (\text{C11})$$

By using the projections of Eq. (C9) we straightforwardly get

$$\begin{aligned} \rho_e(\mathbf{R}, \mathbf{R}') &= \psi_i(\mathbf{R}) \psi_i^*(\mathbf{R}') e^{i[\Phi(\mathbf{R}_t) - \Phi(\mathbf{R}'_t)]} \\ &\times e^{-(1/2)[\Delta(\mathbf{R}_t, \mathbf{R}_t) + \Delta(\mathbf{R}'_t, \mathbf{R}'_t)]} \\ &\times \sum_{n=0}^{\infty} \frac{1}{n!} \left[\int d\xi T(\mathbf{R}, \xi) T^*(\mathbf{R}', \xi) \right]^n \end{aligned} \quad (\text{C12})$$

which can be cast as

$$\begin{aligned} \rho_e(\mathbf{R}, \mathbf{R}') &= \psi_i(\mathbf{R}) \psi_i^*(\mathbf{R}') \\ &\times e^{i[\Phi(\mathbf{R}_t) - \Phi(\mathbf{R}'_t)] - (1/2)[\Delta(\mathbf{R}_t, \mathbf{R}_t) + \Delta(\mathbf{R}'_t, \mathbf{R}'_t)]} \\ &\times e^{\Delta(\mathbf{R}, \mathbf{R}')}, \end{aligned} \quad (\text{C13})$$

where we have summed the power series and we have used the integral

$$\int d\xi T(\mathbf{R}, \xi) T^*(\mathbf{R}', \xi) = \Delta(\mathbf{R}, \mathbf{R}') \quad (\text{C14})$$

which is a simple consequence of Eqs. (C4) and (A15). Since $\psi_i(\mathbf{R}) \psi_i^*(\mathbf{R}')$ is the density matrix of the fully

coherent initial electron state, it is convenient to write Eq. (C13) as

$$\rho_e(\mathbf{R}, \mathbf{R}') = \psi_i(\mathbf{R}) \psi_i^*(\mathbf{R}') \gamma(\mathbf{R}, \mathbf{R}') \quad (\text{C15})$$

where

$$\begin{aligned} \gamma(\mathbf{R}, \mathbf{R}') &= e^{i[\Phi(\mathbf{R}_t) - \Phi(\mathbf{R}'_t)] - (1/2)[\Delta(\mathbf{R}_t, \mathbf{R}_t) + \Delta(\mathbf{R}'_t, \mathbf{R}'_t)]} \\ &\times e^{\Delta(\mathbf{R}_t + (R_v - R'_v) \mathbf{u}_v, \mathbf{R}'_t)} \end{aligned} \quad (\text{C16})$$

quantifies the decoherence of the electron produced by its interaction with the chiral medium. Note that we have used Eq. (B27) to make explicit the dependence of $\Delta(\mathbf{R}, \mathbf{R}')$ on the difference of R_v and R'_v which is also true for γ , that is,

$$\gamma(\mathbf{R}, \mathbf{R}') = \gamma(\mathbf{R}_t + (R_v - R'_v) \mathbf{u}_v, \mathbf{R}'_t). \quad (\text{C17})$$

Note that $\gamma(\mathbf{R}, \mathbf{R}) = 1$ so that $\rho_e(\mathbf{R}, \mathbf{R}) = |\psi_i(\mathbf{R})|^2$, in agreement with the normalization condition

$$\text{Tr}(\hat{\rho}_e) = 1. \quad (\text{C18})$$

APPENDIX D: ELECTRON TRANSVERSE MOMENTUM AND ENERGY DISTRIBUTIONS

The reduced density matrix derived in Appendix C fully describes the state of the electron after its interaction with the chiral film. We here extract from it the electron energy and transverse momentum distribution which is routinely measured in standard electron microscopes (momentum-resolved energy-loss spectroscopy). We start by considering the electron states $|\mathbf{P}_t, E\rangle$ of definite transverse momentum \mathbf{P}_t and energy E , whose wave functions are

$$\langle \mathbf{R} | \mathbf{P}_t, E \rangle = \frac{1}{2\pi\hbar\sqrt{\ell}} e^{(i/\hbar)\mathbf{P}_t \cdot \mathbf{R}_t} e^{i(E/\hbar V)R_v}, \quad (\text{D1})$$

where ℓ is the longitudinal quantization length and $E = (\hbar V/\ell)2\pi m$, with m integer. These states are an orthonormal basis since

$$\int d^2\mathbf{P}_t \sum_E |\mathbf{P}_t, E\rangle \langle \mathbf{P}_t, E| = I, \quad (\text{D2})$$

$$\langle \mathbf{P}_t, E | \mathbf{P}'_t, E' \rangle = \delta(\mathbf{P}_t - \mathbf{P}'_t) \delta_{E, E'}, \quad (\text{D3})$$

and the continuum limit is obtained at the end of the calculations by letting $\ell \rightarrow +\infty$ and by using the relation

$$\sum_E \rightarrow \frac{\ell}{2\pi\hbar V} \int dE. \quad (\text{D4})$$

By inserting the completeness relation [Eq. (D2)] into the reduced density matrix normalization condition [Eq. (C18)] we get

$$1 = \int d^2\mathbf{P}_t \sum_E \frac{1}{(2\pi\hbar)^2 \ell} \int d^3\mathbf{R}' \int d^3\mathbf{R} e^{-(i/\hbar)\mathbf{P}_t \cdot (\mathbf{R}_t - \mathbf{R}')_t} e^{-i(E/\hbar)V(R_v - R'_v)} \rho_e(\mathbf{R}, \mathbf{R}'). \quad (\text{D5})$$

Since the impinging electron has energy E_i , we set for its initial wave function

$$\psi_i(\mathbf{R}) = \frac{1}{\sqrt{\ell}} \phi_i(\mathbf{R}_t) e^{i(E_i/\hbar V)R_v}, \quad (\text{D6})$$

where $\phi_i(\mathbf{R}_t)$ is an arbitrary transverse profile normalized as $\int d^2\mathbf{R}_t |\phi_i(\mathbf{R})|^2 = 1$; accordingly, by using Eqs. (C15) and (D6), Eq. (D5) can be written as

$$\begin{aligned} 1 &= \int d^2\mathbf{P}_t \frac{1}{(2\pi\hbar)^2} \int d^2\mathbf{R}_t \int d^2\mathbf{R}' e^{-(i/\hbar)\mathbf{P}_t \cdot (\mathbf{R}_t - \mathbf{R}')_t} \phi_i(\mathbf{R}_t) \phi_i^*(\mathbf{R}'_t) \\ &\times \sum_E \frac{1}{\ell^2} \int_{-\ell/2}^{\ell/2} dR_v \int_{-\ell/2}^{\ell/2} dR'_v e^{-i(E - E_i/\hbar V)(R_v - R'_v)} \gamma(\mathbf{R}_t + (R_v - R'_v) \mathbf{u}_v, \mathbf{R}'_t). \end{aligned} \quad (\text{D7})$$

After introducing the variable $Q = R_v - R'_v$ and noting that the relation

$$\int_{-\ell/2}^{\ell/2} dR_v \int_{-\ell/2}^{\ell/2} dR'_v F(R_v - R'_v) = \int_{-\ell}^{\ell} dQ (\ell - |Q|) F(Q) \quad (\text{D8})$$

holds for any function $F(R_v - R'_v)$, the continuum limit of Eq. (D7) can easily be evaluated with the help of Eq. (D4) as

$$1 = \int d^2\mathbf{P}_t \int dE \frac{d\mathcal{P}}{d^2\mathbf{P}_t dE}, \quad (\text{D9})$$

where

$$\frac{d\mathcal{P}}{d^2\mathbf{P}_t dE} = \frac{1}{(2\pi\hbar)^3 V} \int d^2\mathbf{R}_t \int d^2\mathbf{R}'_t \int dQ e^{-(i/\hbar)\mathbf{P}_t \cdot (\mathbf{R}_t - \mathbf{R}'_t)} e^{-i(E - E_i/\hbar V)Q} \phi_i(\mathbf{R}_t) \phi_i^*(\mathbf{R}'_t) \gamma(\mathbf{R}_t + Q\mathbf{u}_v, \mathbf{R}'_t) \quad (\text{D10})$$

is the transverse momentum and energy probability distribution of the electron after the interaction with the chiral film. By integrating this expression over E we get the transverse momentum probability distribution

$$\frac{d\mathcal{P}}{d^2\mathbf{P}_t} = \frac{1}{(2\pi\hbar)^2} \int d^2\mathbf{R}_t \int d^2\mathbf{R}'_t e^{-(i/\hbar)\mathbf{P}_t \cdot (\mathbf{R}_t - \mathbf{R}'_t)} \phi_i(\mathbf{R}_t) \phi_i^*(\mathbf{R}'_t) \gamma(\mathbf{R}_t, \mathbf{R}'_t). \quad (\text{D11})$$

It is crucial here to evaluate the transverse momentum mean value and variance. We start by decomposing transverse position and momentum into their orthogonal components, $\mathbf{R}_t = R_1 \mathbf{u}_1 + R_2 \mathbf{u}_2$ and $\mathbf{P}_t = P_1 \mathbf{u}_1 + P_2 \mathbf{u}_2$, where \mathbf{u}_1 and \mathbf{u}_2 are orthogonal unit vectors spanning the transverse plane and we consider the m th-order moments

$$\langle P_j^m \rangle = \int d^2\mathbf{P}_t \frac{d\mathcal{P}}{d^2\mathbf{P}_t} P_j^m. \quad (\text{D12})$$

By using the distribution of Eq. (D11) we get

$$\langle P_j^m \rangle = \int d^2\mathbf{R}_t \int d^2\mathbf{R}'_t \left[\left(-\frac{\hbar}{i} \frac{\partial}{\partial R_j} \right)^m \delta(\mathbf{R}_t - \mathbf{R}'_t) \right] \phi_i(\mathbf{R}_t) \phi_i^*(\mathbf{R}'_t) \gamma(\mathbf{R}_t, \mathbf{R}'_t) \quad (\text{D13})$$

which can be written, after integrating by parts n times and performing the integration over \mathbf{R}'_t and Q with the help of the delta functions, as

$$\langle P_j^m \rangle = \int d^2\mathbf{R}_t \phi_i^*(\mathbf{R}_t) \left\{ \hat{P}_j^m [\phi_i(\mathbf{R}_t) \gamma(\mathbf{R}_t, \mathbf{R}'_t)] \right\}_{\mathbf{R}'_t = \mathbf{R}_t} \quad (\text{D14})$$

where we have introduced the transverse momentum operator $\hat{P}_j = (\hbar/i)(\partial/\partial R_j)$. For $m = 1$ and $m = 2$ this relation readily provides the transverse momentum mean value

$$\langle P_j \rangle = \int d^2 \mathbf{R}_t \phi_i^* \hat{P}_j \phi_i + \int d^2 \mathbf{R}_t |\phi_i|^2 \left(\hat{P}_j \Theta \right)_{\mathbf{R}'_t = \mathbf{R}_t} \quad (D15)$$

and variance

$$\begin{aligned} \langle P_j^2 \rangle - \langle P_j \rangle^2 &= \left[\int d^2 \mathbf{R}_t \phi_i^* \hat{P}_j^2 \phi_i - \left(\int d^2 \mathbf{R}_t \phi_i^* \hat{P}_j \phi_i \right)^2 \right] \\ &+ 2 \left\{ \int d^2 \mathbf{R}_t \left(\phi_i^* \hat{P}_j \phi_i \right) \left(\hat{P}_j \Theta \right)_{\mathbf{R}'_t = \mathbf{R}_t} - \left(\int d^2 \mathbf{R}_t \phi_i^* \hat{P}_j \phi_i \right) \left[\int d^2 \mathbf{R}_t |\phi_i|^2 \left(\hat{P}_j \Theta \right)_{\mathbf{R}'_t = \mathbf{R}_t} \right] \right\} \\ &+ \left\{ \int d^2 \mathbf{R}_t |\phi_i|^2 \left[\left(\hat{P}_j \Theta \right)^2 + \hat{P}_j^2 \Theta \right]_{\mathbf{R}'_t = \mathbf{R}_t} - \left[\int d^2 \mathbf{R}_t |\phi_i|^2 \left(\hat{P}_j \Theta \right)_{\mathbf{R}'_t = \mathbf{R}_t} \right]^2 \right\}, \end{aligned} \quad (D16)$$

where we have set

$$\Theta(\mathbf{R}_t, \mathbf{R}'_t) = \log \gamma(\mathbf{R}_t, \mathbf{R}'_t). \quad (D17)$$

Note that both transverse momentum mean value and variance remarkably turn out to be the sum of their initial contribution plus terms (containing Θ) resulting from the interaction with the chiral medium.

APPENDIX E: GREEN'S TENSOR COMPONENT ALONG THE ELECTRON VELOCITY

In Fig. 5 (left) we have sketched the electron-chiral film mutual geometry, while in Fig. 5 (right), for the sake of clarity, we have summarized the quantities used in the analysis below. In order to evaluate the Green's tensor component $\mathcal{G}_{\omega xx}(\mathbf{r}, \mathbf{r}') = \mathbf{e}_x \cdot \mathcal{G}_\omega(\mathbf{r}, \mathbf{r}') \mathbf{e}_x$ in the vacuum half-space we start by noting that an elementary current density $\mathbf{J}_\omega(\mathbf{r}) = J_\omega \delta(\mathbf{r} - \mathbf{r}') \mathbf{e}_x$ located in a vacuum ($z' < 0$) produces at $z < 0$ the field

$$\mathbf{E}_\omega(\mathbf{r}) = (i\omega\mu_0 J_\omega) \mathcal{G}_\omega(\mathbf{r}, \mathbf{r}') \mathbf{e}_x = \mathbf{E}_\omega^{(0)}(\mathbf{r}) + \mathbf{E}_\omega^{(r)}(\mathbf{r}), \quad (E1)$$

where $\mathbf{E}_\omega^{(0)}$ is the free-space field produced by the elementary current

$$\mathbf{E}_\omega^{(0)} = (i\omega\mu_0 J_\omega) \left(1 + \frac{\nabla \nabla \cdot}{k_\omega^2 \epsilon_1} \right) \frac{e^{ik_\omega \sqrt{\epsilon_1} |\mathbf{r} - \mathbf{r}'|}}{4\pi |\mathbf{r} - \mathbf{r}'|} \mathbf{e}_x \quad (E2)$$

and $\mathbf{E}_\omega^{(r)}$ is the field reflected by the chiral film interface [see Fig. 5 (left)]. To evaluate the reflected field it is convenient to cast the free-space field as

$$\mathbf{E}_\omega^{(0)} = (i\omega\mu_0 J_\omega) \frac{i}{8\pi^2} \int d^2 \mathbf{k}_\parallel e^{i\mathbf{k}_\parallel \cdot (\mathbf{r}_\parallel - \mathbf{r}'_\parallel)} \frac{e^{ik_{1z}|z-z'|}}{k_{1z}} \left\{ \left(-\frac{k_y}{k_\parallel} \right) \mathbf{u}_S + \left(\frac{k_{1z}^2 k_x}{k_\parallel k_\omega^2 \epsilon_1} \right) \left[\mathbf{u}_P - \frac{k_\parallel}{k_{1z}} \text{sgn}(z - z') \mathbf{e}_z \right] \right\} \quad (E3)$$

where we have used the Weyl representation of the spherical wave

$$\frac{e^{ik_\omega \sqrt{\epsilon_1} |\mathbf{r} - \mathbf{r}'|}}{|\mathbf{r} - \mathbf{r}'|} = \frac{i}{2\pi} \int d^2 \mathbf{k}_\parallel e^{i\mathbf{k}_\parallel \cdot (\mathbf{r}_\parallel - \mathbf{r}'_\parallel)} \frac{e^{ik_{1z}|z-z'|}}{k_{1z}}. \quad (E4)$$

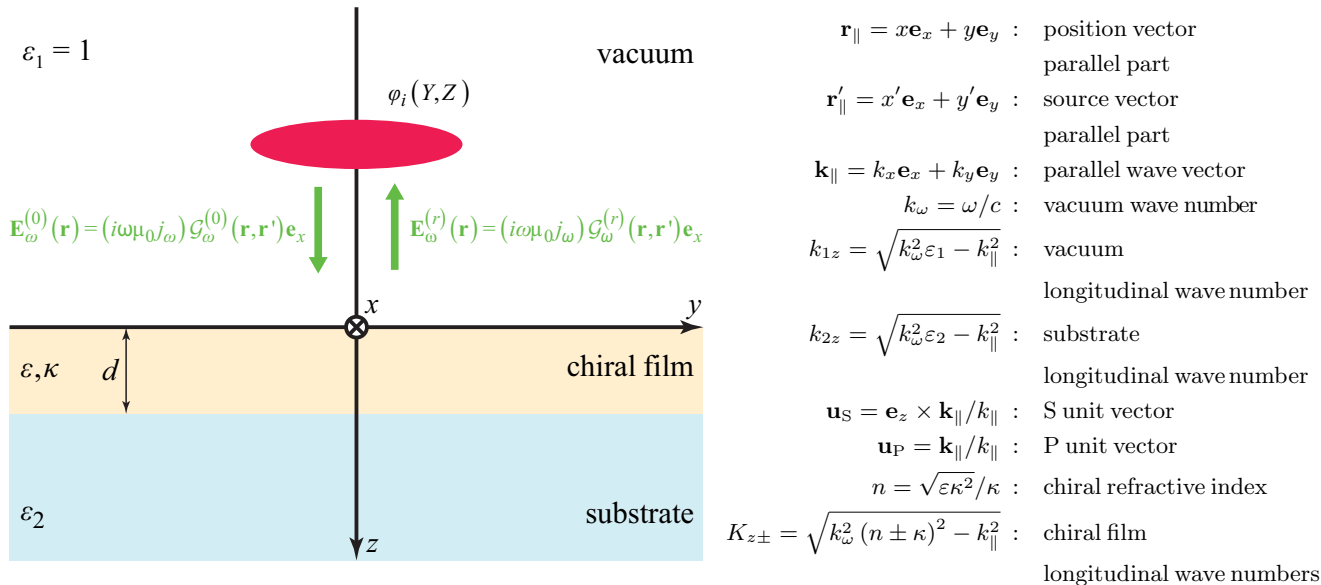


FIG. 5. (Left) Geometry of the interaction between the aloof electron traveling in a vacuum parallel to the x axis near the chiral film deposited onto the substrate. The red spot shows the initial electron wave-function transverse profile $\phi_i(Y, Z)$, while the green arrows sketch the vacuum and reflected fields, $\mathbf{E}_{\omega}^{(0)}$ and $\mathbf{E}_{\omega}^{(r)}$, used to evaluate the Green's tensor component along the electron velocity. Right List of quantities used in the evaluation.

Now in Ref.[3] it has been shown that an incident field

$$\mathbf{E}_{\omega}^{(i)} = \int d^2\mathbf{k}_{\parallel} e^{i\mathbf{k}_{\parallel} \cdot \mathbf{r}} e^{ik_{1z}z} \left[U_S^{(i)} \mathbf{u}_S + U_P^{(i)} \left(\mathbf{u}_P - \frac{k_{\parallel}}{k_{1z}} \mathbf{e}_z \right) \right] \quad (\text{E5})$$

impinging onto the chiral film/substrate composite produces at $z < 0$ the reflected field

$$\mathbf{E}_{\omega}^{(r)} = \int d^2\mathbf{k}_{\parallel} e^{i\mathbf{k}_{\parallel} \cdot \mathbf{r}} e^{-ik_{1z}z} \left[\left(R_{SS} U_S^{(i)} + n R_{SP} U_P^{(i)} \right) \mathbf{u}_S + \left(n R_{PS} U_S^{(i)} + R_{PP} U_P^{(i)} \right) \left(\mathbf{u}_P + \frac{k_{\parallel}}{k_{1z}} \mathbf{e}_z \right) \right] \quad (\text{E6})$$

in which the reflection matrix is given by

$$\begin{pmatrix} R_{SS} & n R_{SP} \\ n R_{PS} & R_{PP} \end{pmatrix} = \begin{pmatrix} 1 & 0 \\ 0 & -1 \end{pmatrix} (M^{(1)} - M^{(2)}) (M^{(1)} + M^{(2)})^{-1}, \quad (\text{E7})$$

where

$$\begin{aligned} M^{(1)} &= \begin{pmatrix} \left(C_+ + \frac{k_{2z}}{ik_{\omega}} S_+^{(1)} \right) & n \left(\frac{k_{\omega}\varepsilon_2}{ik_{2z}\varepsilon} C_- - S_-^{(1)} \right) \\ n \frac{ik_{1z}}{k_{\omega}\varepsilon_1} \left(C_- + \frac{k_{2z}}{ik_{\omega}} S_-^{(1)} \right) & \varepsilon \frac{ik_{1z}}{k_{\omega}\varepsilon_1} \left(\frac{k_{\omega}\varepsilon_2}{ik_{2z}\varepsilon} C_+ - S_+^{(1)} \right) \end{pmatrix}, \\ M^{(2)} &= \begin{pmatrix} \frac{k_{\omega}}{ik_{1z}} \left(\frac{ik_{2z}}{k_{\omega}} C_+ + S_+^{(2)} \right) & n \frac{k_{\omega}}{ik_{1z}} \left(C_- + \frac{k_{\omega}\varepsilon_2}{ik_{2z}\varepsilon} S_-^{(2)} \right) \\ n \frac{1}{\varepsilon} \left(\frac{ik_{2z}}{k_{\omega}} C_- + S_-^{(2)} \right) & \left(C_+ + \frac{k_{\omega}\varepsilon_2}{ik_{2z}\varepsilon} S_+^{(2)} \right) \end{pmatrix}, \end{aligned} \quad (\text{E8})$$

and

$$\begin{aligned} C_{\pm} &= \frac{1}{2} [\cos(K_{z+}d) \pm \cos(K_{z-}d)], \\ S_{\pm}^{(1)} &= \frac{1}{2} \left[\frac{k_{\omega}(n+\kappa)}{K_{z+}n} \sin(K_{z+}d) \pm \frac{k_{\omega}(n-\kappa)}{K_{z-}n} \sin(K_{z-}d) \right], \\ S_{\pm}^{(2)} &= \frac{1}{2} \left[\frac{K_{z+}n}{k_{\omega}(n+\kappa)} \sin(K_{z+}d) \pm \frac{K_{z-}n}{k_{\omega}(n-\kappa)} \sin(K_{z-}d) \right]. \end{aligned} \quad (\text{E9})$$

It is worth noting that the reflection coefficients R_{IJ} defined in Eq. (E7) are left invariant by chirality reversal $\kappa \rightarrow -\kappa$, as can easily be proved with help of the matrices $M^{(j)}$ of Eqs. (E8). The only term affected by chirality reversal is the chiral refractive index $n = \sqrt{\varepsilon\kappa^2}/\kappa$ whose sign is switched by the reversal.

Since along the strip $z' < z < 0$ the free-space field in Eq. (E3) has the same structure of the field in Eq. (E5) with S and P amplitudes

$$\begin{aligned} U_S^{(i)} &= (i\omega\mu_0J_{\omega}) \frac{i}{8\pi^2} e^{-ik_{\parallel}\cdot\mathbf{r}'} \frac{e^{-ik_{1z}z'}}{k_{1z}} \left(-\frac{k_y}{k_{\parallel}} \right), \\ U_P^{(i)} &= (i\omega\mu_0J_{\omega}) \frac{i}{8\pi^2} e^{-ik_{\parallel}\cdot\mathbf{r}'} \frac{e^{-ik_{1z}z'}}{k_{1z}} \left(\frac{k_{1z}^2 k_x}{k_{\parallel} k_{\omega}^2 \varepsilon_1} \right), \end{aligned} \quad (\text{E10})$$

the reflected field is readily given by Eq. (E6) as

$$\begin{aligned} \mathbf{E}_{\omega}^{(r)} &= (i\omega\mu_0J_{\omega}) \frac{i}{8\pi^2} \int d^2\mathbf{k}_{\parallel} e^{i\mathbf{k}_{\parallel}\cdot(\mathbf{r}_{\parallel}-\mathbf{r}'_{\parallel})} \frac{e^{-ik_{1z}(z+z')}}{k_{1z}} \left[\left(-R_{SS} \frac{k_y}{k_{\parallel}} + nR_{SP} \frac{k_{1z}^2 k_x}{k_{\parallel} k_{\omega}^2 \varepsilon_1} \right) \mathbf{u}_S \right. \\ &\quad \left. + \left(-nR_{PS} \frac{k_y}{k_{\parallel}} + R_{PP} \frac{k_{1z}^2 k_x}{k_{\parallel} k_{\omega}^2 \varepsilon_1} \right) \left(\mathbf{u}_P + \frac{k_{\parallel}}{k_{1z}} \mathbf{e}_z \right) \right]. \end{aligned} \quad (\text{E11})$$

Projecting the field in Eq. (E1) onto the x axis and using Eqs. (E3) and (E11) we get the xx component $\mathcal{G}_{\omega xx} = \mathbf{e}_x \cdot \mathcal{G}_{\omega} \mathbf{e}_x$ of the Green's tensor,

$$\mathcal{G}_{\omega xx}(\mathbf{r}, \mathbf{r}') = \mathcal{G}_{\omega xx}^{(0)}(\mathbf{r}, \mathbf{r}') + \mathcal{G}_{\omega xx}^{(r)}(\mathbf{r}, \mathbf{r}'), \quad (\text{E12})$$

where

$$\begin{aligned} \mathcal{G}_{\omega xx}^{(0)}(\mathbf{r}, \mathbf{r}') &= \frac{i}{8\pi^2} \int d^2\mathbf{k}_{\parallel} e^{i\mathbf{k}_{\parallel}\cdot(\mathbf{r}_{\parallel}-\mathbf{r}'_{\parallel})} \frac{e^{ik_{1z}|z-z'|}}{k_{1z}} \left(1 - \frac{k_x^2}{k_{\omega}^2 \varepsilon_1} \right), \\ \mathcal{G}_{\omega xx}^{(r)}(\mathbf{r}, \mathbf{r}') &= \frac{i}{8\pi^2} \int d^2\mathbf{k}_{\parallel} e^{i\mathbf{k}_{\parallel}\cdot(\mathbf{r}_{\parallel}-\mathbf{r}'_{\parallel})} \frac{e^{-ik_{1z}(z+z')}}{k_{1z}} \left[\left(R_{SS} \frac{k_y^2}{k_{\parallel}^2} + R_{PP} \frac{k_{1z}^2 k_x^2}{k_{\omega}^2 \varepsilon_1 k_{\parallel}^2} \right) - n \left(R_{SP} \frac{k_{1z}^2}{k_{\omega}^2 \varepsilon_1} + R_{PS} \right) \frac{k_x k_y}{k_{\parallel}^2} \right] \end{aligned} \quad (\text{E13})$$

are the xx components of the free-space and reflected parts of the Green's tensor, $\mathcal{G}_{\omega}^{(0)}(\mathbf{r}, \mathbf{r}')$ and $\mathcal{G}_{\omega}^{(r)}(\mathbf{r}, \mathbf{r}')$.

Mirror asymmetry of the Green's tensor can easily be checked since, for the reflection $\mathcal{R} = \mathbf{e}_x \mathbf{e}_x - \mathbf{e}_y \mathbf{e}_y + \mathbf{e}_z \mathbf{e}_z$ through the $\pi = z-x$ plane, from Eqs. (E13) we straightforwardly get

$$\begin{aligned} \mathcal{G}_{\omega xx}^{(0)}(\mathcal{R}\mathbf{r}, \mathcal{R}\mathbf{r}') - \mathcal{G}_{\omega xx}^{(0)}(\mathbf{r}, \mathbf{r}') &= 0, \\ \mathcal{G}_{\omega xx}^{(r)}(\mathcal{R}\mathbf{r}, \mathcal{R}\mathbf{r}') - \mathcal{G}_{\omega xx}^{(r)}(\mathbf{r}, \mathbf{r}') &= 2n \frac{i}{8\pi^2} \int d^2\mathbf{k}_{\parallel} e^{i\mathbf{k}_{\parallel}\cdot(\mathbf{r}_{\parallel}-\mathbf{r}'_{\parallel})} \frac{e^{-ik_{1z}(z+z')}}{k_{1z}} \left(R_{SP} \frac{k_{1z}^2}{k_{\omega}^2 \varepsilon_1} + R_{PS} \right) \frac{k_x k_y}{k_{\parallel}^2}, \end{aligned} \quad (\text{E14})$$

clearly agreeing with Eq. (9). Note that Green's tensor mirror asymmetry is here due to the mixing reflection coefficients R_{SP} and R_{PS} which are also responsible for the mirror optical activity (MOA) effect discussed in Refs. [3,4].

APPENDIX F: MIRROR-SYMMETRY BREAKING OF THE ELECTRON QUANTUM PROPERTIES

We evaluate here the phase factor $\Phi(\mathbf{R})$ and the fundamental quantity $\Delta(\mathbf{R}, \mathbf{R}')$ for $Z < 0$ and $Z' < 0$. Since the electron velocity is parallel to the x axis, the t and v parts of \mathbf{R} and \mathbf{R}' are (see Eq. (B17))

$$\begin{aligned}\mathbf{R}_t &= Y\mathbf{e}_y + Z\mathbf{e}_z, & R_v &= X, \\ \mathbf{R}'_t &= Y'\mathbf{e}_y + Z'\mathbf{e}_z, & R'_v &= X',\end{aligned}\tag{F1}$$

and accordingly, from the first part of Eqs. (B23) and from (B25), we have

$$\begin{aligned}\Phi(\mathbf{R}_t) &= \frac{4\alpha}{c} \text{Im} \int_0^{+\infty} d\omega \int_{-\infty}^{+\infty} dq \int_{-\infty}^q dq' e^{i(\omega/V)(q-q')} \text{Im} [\mathcal{G}_{\omega xx}(\mathbf{r}, \mathbf{r}')]_{\substack{\mathbf{r}=q\mathbf{e}_x+Y\mathbf{e}_y+Z\mathbf{e}_z \\ \mathbf{r}'=q'\mathbf{e}_x+Y\mathbf{e}_y+Z\mathbf{e}_z}}, \\ \Delta(\mathbf{R}, \mathbf{R}') &= \frac{4\alpha}{c} \int_0^{\infty} d\omega e^{-i(\omega/V)(X-X')} \int_{-\infty}^{+\infty} dq \int_{-\infty}^{+\infty} dq' e^{i(\omega/V)(q-q')} \text{Im} [\mathcal{G}_{\omega xx}(\mathbf{r}, \mathbf{r}')]_{\substack{\mathbf{r}=q\mathbf{e}_x+Y\mathbf{e}_y+Z\mathbf{e}_z \\ \mathbf{r}'=q'\mathbf{e}_x+Y'\mathbf{e}_y+Z'\mathbf{e}_z}}.\end{aligned}\tag{F2}$$

By exploiting the rotational invariance of the vacuum longitudinal wave number $k_{1z}(k_{\parallel}^2)$ and of the reflection coefficients $R_{IJ}(k_{\parallel}^2)$, from Eqs. (E12) and (E13) we get the imaginary part of the xx component of the Green's tensor

$$\text{Im} [\mathcal{G}_{\omega xx}(\mathbf{r}, \mathbf{r}')] = \frac{1}{8\pi^2} \int d^2\mathbf{k}_{\parallel} e^{i\mathbf{k}_{\parallel} \cdot (\mathbf{r}_{\parallel} - \mathbf{r}'_{\parallel})} \text{Re} \left[\frac{e^{ik_{1z}|z-z'|}}{k_{1z}} \left(1 - \frac{k_x^2}{k_{\omega}^2 \epsilon_1} \right) + \frac{e^{-ik_{1z}(z+z')}}{k_{1z}} \Upsilon \right] \tag{F3}$$

where

$$\Upsilon(\omega, \mathbf{k}_{\parallel}) = \left(R_{SS} \frac{k_y^2}{k_{\parallel}^2} + R_{PP} \frac{k_{1z}^2}{k_{\omega}^2 \epsilon_1} \frac{k_x^2}{k_{\parallel}^2} \right) - n \left(R_{SP} \frac{k_{1z}^2}{k_{\omega}^2 \epsilon_1} + R_{PS} \right) \frac{k_x k_y}{k_{\parallel}^2}, \tag{F4}$$

which, inserted into Eqs. (F2), yields

$$\begin{aligned}\Phi(\mathbf{R}_t) &= \frac{\alpha}{2\pi^2 c} \int_0^{+\infty} d\omega \int d^2\mathbf{k}_{\parallel} \left[\text{Im} \int_{-\infty}^{+\infty} dq \int_{-\infty}^q dq' e^{i(k_x+(\omega/V))(q-q')} \right] \text{Re} \left[\frac{1}{k_{1z}} \left(1 - \frac{k_x^2}{k_{\omega}^2 \epsilon_1} \right) + \frac{e^{-i2k_{1z}Z}}{k_{1z}} \Upsilon \right], \\ \Delta(\mathbf{R}, \mathbf{R}') &= \frac{\alpha}{2\pi^2 c} \int_0^{\infty} d\omega e^{-i(\omega/V)(X-X')} \int d^2\mathbf{k}_{\parallel} e^{ik_y(Y-Y')} \left[\int_{-\infty}^{+\infty} dq \int_{-\infty}^{+\infty} dq' e^{i(k_x+(\omega/V))(q-q')} \right] \\ &\quad \times \text{Re} \left[\frac{e^{ik_{1z}|Z-Z'|}}{k_{1z}} \left(1 - \frac{k_x^2}{k_{\omega}^2 \epsilon_1} \right) + \frac{e^{-ik_{1z}(Z+Z')}}{k_{1z}} \Upsilon \right].\end{aligned}\tag{F5}$$

Note that the free-space contribution to Φ is independent of \mathbf{R}_t and so we henceforth neglect it since it provides an unobservable phase factor in the reduced density matrix. The integrals over q' can be analytically evaluated as

$$\begin{aligned}\text{Im} \int_{-\infty}^q dq' e^{i(k_x+(\omega/V))(q-q')} &= \text{p.v.} \frac{1}{k_x + (\omega/V)}, \\ \int_{-\infty}^{+\infty} dq' e^{i(k_x+(\omega/V))(q-q')} &= 2\pi \delta \left(k_x + \frac{\omega}{V} \right),\end{aligned}\tag{F6}$$

where p.v. stands for the Cauchy principal value, while the remaining integral over q can be replaced by the effective electron path length which can be approximated by L , the longitudinal length of the chiral film (see Fig. 1 in the main

text). By inserting these integrals into Eqs. (F5) we get

$$\begin{aligned}\Phi(\mathbf{R}_t) &= \frac{L\alpha}{2\pi^2 c} \text{p.v.} \int_0^{+\infty} d\omega \int d^2 \mathbf{k}_{\parallel} \frac{1}{k_x + (\omega/V)} \text{Re} \left(\frac{e^{-i2k_{1z}Z}}{k_{1z}} \Upsilon \right), \\ \Delta(\mathbf{R}, \mathbf{R}') &= \frac{L\alpha}{\pi c} \int_0^{\infty} d\omega \int_{-\infty}^{+\infty} dk_y e^{-i(\omega/V)(X-X')} e^{ik_y(Y-Y')} \frac{e^{\sqrt{k_{\omega}^2[(1/\beta^2)-\varepsilon_1]+k_y^2}(Z+Z')}}{\sqrt{k_{\omega}^2[(1/\beta^2)-\varepsilon_1]+k_y^2}} \text{Im}(\Upsilon)_{k_x=-(\omega/V)}. \end{aligned}\quad (\text{F7})$$

Note that the free-space part of the Green's tensor does not affect $\Delta(\mathbf{R}, \mathbf{R}')$ since its contribution in the curly bracket in the second part of Eqs. (F5) is purely imaginary because $k_{1z} = i\sqrt{k_{\omega}^2[(1/\beta^2)-\varepsilon_1]+k_y^2}$ for $k_x = -\omega/V$. In addition, due to the planar geometry of the chiral film, the phase factor Φ is a function only of Z , while $\Delta(\mathbf{R}, \mathbf{R}')$ only depends on $X - X'$, $Y - Y'$, and $Z + Z'$. Equations (F7) enable the evaluation of the reduced density matrix of Eq. (C15).

The Green's tensor component xx is not symmetric under mirror reflections, as discussed above, and this entails that the aloof electron-chiral film interaction has broken mirror symmetry. In order to discuss this crucial point, from the second part of Eqs. (F7) it is convenient to note that the decomposition

$$\Delta(\mathbf{R}, \mathbf{R}') = \Delta_S(X - X', Y - Y', Z + Z') + i\Delta_A(X - X', Y - Y', Z + Z') \quad (\text{F8})$$

holds, in which

$$\begin{aligned}\Delta_S(\tilde{X}, \tilde{Y}, \tilde{Z}) &= \frac{L\alpha}{\pi c} \int_0^{\infty} d\omega e^{-i(\omega/V)\tilde{X}} \int_{-\infty}^{+\infty} dk_y \cos(k_y \tilde{Y}) \\ &\times \frac{e^{\sqrt{k_{\omega}^2[(1/\beta^2)-\varepsilon_1]+k_y^2}\tilde{Z}}}{\sqrt{k_{\omega}^2[(1/\beta^2)-\varepsilon_1]+k_y^2}} \text{Im} \left(R_{SS} \frac{k_y^2}{k_{\parallel}^2} + R_{PP} \frac{k_{1z}^2}{k_0^2 \varepsilon_1} \frac{k_x^2}{k_{\parallel}^2} \right)_{k_x=-(\omega/V)}, \\ \Delta_A(\tilde{X}, \tilde{Y}, \tilde{Z}) &= \frac{L\alpha}{\pi c} \int_0^{\infty} d\omega e^{-i(\omega/V)\tilde{X}} \int_{-\infty}^{+\infty} dk_y \sin(k_y \tilde{Y}) \\ &\times \frac{e^{\sqrt{k_{\omega}^2[(1/\beta^2)-\varepsilon_1]+k_y^2}\tilde{Z}}}{\sqrt{k_{\omega}^2[(1/\beta^2)-\varepsilon_1]+k_y^2}} \text{Im} \left[-n \left(R_{SP} \frac{k_{1z}^2}{k_0^2 \varepsilon_1} + R_{PS} \right) \frac{k_x k_y}{k_{\parallel}^2} \right]_{k_x=-(\omega/V)} \end{aligned}\quad (\text{F9})$$

are symmetric and antisymmetric under the reflection through the x - z plane, respectively, since

$$\begin{aligned}\Delta_S(\tilde{X}, -\tilde{Y}, \tilde{Z}) &= \Delta_S(\tilde{X}, \tilde{Y}, \tilde{Z}), \\ \Delta_A(\tilde{X}, -\tilde{Y}, \tilde{Z}) &= -\Delta_A(\tilde{X}, \tilde{Y}, \tilde{Z}).\end{aligned}\quad (\text{F10})$$

Note that Δ_A only contains the mixing reflection coefficients R_{SP} and R_{PS} and accordingly its sign is switched by chirality reversal $\kappa \rightarrow -\kappa$ since it is proportional to the chiral refractive index n . Equation (F8) shows that the mirror symmetry of Δ is broken by MOA, enabling the decoherence factor of Eq. (C16) to be written as

$$\gamma(\mathbf{R}, \mathbf{R}') = e^{i[\Phi(Z) - \Phi(Z')]} e^{\Delta_S(X - X', Y - Y', Z + Z') - (1/2)[\Delta_S(0, 0, 2Z) + \Delta_S(0, 0, 2Z')]} e^{i\Delta_A(X - X', Y - Y', Z + Z')} \quad (\text{F11})$$

which, in agreement with the general case of Eq. (12), evidently has broken mirror symmetry here due to the last exponential factor containing Δ_A . In order to quantify its absolute mirror asymmetry we consider the dimensionless quantity

$$\text{Asym}[\gamma(\mathbf{R}, \mathbf{R}')] = 2 \frac{\gamma(\mathbf{R}, \mathbf{R}') - \gamma(\mathcal{R}\mathbf{R}, \mathcal{R}\mathbf{R}')}{\gamma(\mathbf{R}, \mathbf{R}') + \gamma(\mathcal{R}\mathbf{R}, \mathcal{R}\mathbf{R}')} \quad (\text{F12})$$

which compares $\gamma(\mathbf{R}, \mathbf{R}')$ and its mirror image $\gamma(\mathcal{R}\mathbf{R}, \mathcal{R}\mathbf{R}')$ through the ratio between their difference and their arithmetic average. Inserting Eq. (F11) into Eq. (F12), we obtain

$$\text{Asym}[\gamma(\mathbf{R}, \mathbf{R}')] = 2i \tan [\Delta_A(X - X', Y - Y', Z + Z')], \quad (\text{F13})$$

clearly elucidating that MOA breaks the mirror symmetry of the electron decoherence. Since Δ_A is proportional to L , the absolute asymmetry of the decoherence factor can be enhanced in the presence of long effective interaction lengths. For an initial mirror-symmetric electron wave function [see Eq. (10)], Eq. (F13) also provides the absolute mirror asymmetry of the electron reduced density matrix [see Eq. (C15)].

As discussed in Sec. III of the main text, the electron transverse momentum distribution lacks mirror symmetry in the lateral direction. We here focus on the distribution of the lateral momentum component P_y which is given by $d\mathcal{P}/dP_y = \int dP_z d\mathcal{P}/d^2\mathbf{P}_t$. From Eq. (D11) we straightforwardly get

$$\frac{d\mathcal{P}}{dP_y} = \frac{1}{2\pi\hbar} \int dY \int dY' \int dZ e^{-(i/\hbar)P_y(Y-Y')} \phi_i(Y, Z) \phi_i^*(Y', Z) [\gamma(\mathbf{R}_t, \mathbf{R}'_t)]_{Z'=Z} \quad (\text{F14})$$

which, after using Eq. (F11) and performing the change of integration variables $Y' = Y - \tilde{Y}$, $Z = \tilde{Z}/2$, becomes

$$\frac{d\mathcal{P}}{dP_y} = \frac{1}{4\pi\hbar} \int d\tilde{Y} \int d\tilde{Z} e^{-(i/\hbar)P_y\tilde{Y}} \tilde{\phi}_i(\tilde{Y}, \tilde{Z}) e^{\Delta_S(0, \tilde{Y}, \tilde{Z}) - \Delta_S(0, 0, \tilde{Z})} e^{i\Delta_A(0, \tilde{Y}, \tilde{Z})} \quad (\text{F15})$$

where

$$\tilde{\phi}_i(\tilde{Y}, \tilde{Z}) = \int dY \phi_i(Y, \tilde{Z}/2) \phi_i^*(Y - \tilde{Y}, \tilde{Z}/2) \quad (\text{F16})$$

is the autoconvolution of the initial electron wave function. For the initial mirror-symmetric electron wave function $\phi_i(-Y, Z) = \phi_i(Y, Z)$, the autoconvolution $\tilde{\phi}_i(\tilde{Y}, \tilde{Z})$ is even in \tilde{Y} . Now the real quantities $\Delta_S(0, \tilde{Y}, \tilde{Z}) - \Delta_S(0, 0, \tilde{Z})$ and $\Delta_A(0, \tilde{Y}, \tilde{Z})$ are respectively even and odd in \tilde{Y} , and hence we conclude that $d\mathcal{P}/dP_y$ of Eq. (F15) cannot be either even or odd in P_y since it is the Fourier transform of a function whose parity is indefinite. To explicitly highlight its asymmetry we write Eq. (F15) as

$$\begin{aligned} \frac{d\mathcal{P}}{dP_y} &= \frac{1}{4\pi\hbar} \int d\tilde{Y} \int d\tilde{Z} \tilde{\phi}_i(\tilde{Y}, \tilde{Z}) e^{\Delta_S(0, \tilde{Y}, \tilde{Z}) - \Delta_S(0, 0, \tilde{Z})} \\ &\times \left\{ \underbrace{\cos\left(\frac{1}{\hbar}P_y\tilde{Y}\right) \cos[\Delta_A(0, \tilde{Y}, \tilde{Z})]}_{\text{even in } P_y} + \underbrace{\sin[(1/\hbar)P_y\tilde{Y}] \sin[\Delta_A(0, \tilde{Y}, \tilde{Z})]}_{\text{odd in } P_y} \right\} \end{aligned} \quad (\text{F17})$$

where the even and odd contributions to the transverse momentum distribution are separated. The odd part is entirely due to Δ_A , so that the mirror symmetry of the electron lateral momentum distribution is broken by medium chirality.

As discussed in Sec. III of the main text, the asymmetry of the transverse momentum distribution has the remarkable consequence that the electron gains a net lateral momentum upon scattering. To explicitly discuss this phenomenon for the aloof electron we are considering, we evaluate the mean value and variance of P_y . Using the fact that the impinging electron with mirror-symmetric wave function has no transverse momentum, $\int dY \int dZ \phi_i^*((\hbar/i)(\partial/\partial Y)) \phi_i = 0$, Eqs. (D15) and (D16) with $j = y$ yield, after some algebra,

$$\begin{aligned} \langle P_y \rangle &= \int dY \int dZ |\phi_i|^2 A, \\ \langle P_y^2 \rangle - \langle P_y \rangle^2 &= \int dY \int dZ \phi_i^* \left(\frac{\hbar}{i} \frac{\partial}{\partial Y} \right)^2 \phi_i + \int dY \int dZ |\phi_i|^2 S + \left\{ \int dY \int dZ |\phi_i|^2 A^2 - \left[\int dY \int dZ |\phi_i|^2 A \right]^2 \right\}, \end{aligned} \quad (\text{F18})$$

where

$$\begin{aligned} A(Z) &= \left[\hbar \frac{\partial \Delta_A(0, \tilde{Y}, 2Z)}{\partial \tilde{Y}} \right]_{\tilde{Y}=0}, \\ S(Z) &= \left[-\hbar^2 \frac{\partial^2 \Delta_S(0, \tilde{Y}, 2Z)}{\partial \tilde{Y}^2} \right]_{\tilde{Y}=0}. \end{aligned} \quad (\text{F19})$$

The first part of Eqs. (F18) makes explicit that the mean value of P_y is fully due to medium chirality, as expected, and this is one of the main results of this work. The second part of Eqs. (F18) reveals that the variance of P_y has two contributions that add up to the initial variance $\int dY \int dZ \phi_i^* [(\hbar/i)(\partial/\partial Y)]^2 \phi_i$. The one containing Δ_S (through S) is nonvanishing even in the achiral limit $\Delta_A = 0$ and accounts for the natural momentum distribution reshaping produced by the interaction of the electron with the medium. On the other hand, the contribution containing Δ_A (through A) is entirely produced by medium chirality and it is expected to be very small as compared to the previous one.

- [1] N. Berova, P. L. Polavarapu, K. Nakanishi, and R. W. Woody, *Comprehensive Chiroptical Spectroscopy: Applications in Stereochemical Analysis of Synthetic Compounds, Natural Products, and Biomolecules* (John Wiley & Sons, New York, 2012).
- [2] L. D. Barron, *Molecular Light Scattering and Optical Activity* (Cambridge University Press, Cambridge, 2004).
- [3] A. Ciattoni, Mirror Optical Activity: Nanophotonic Chiral Sensing from Parity Indefiniteness, *Phys. Rev. Appl.* **16**, 034041 (2021).
- [4] A. Ciattoni, Asymmetric Scattering of Mirror-Symmetric Radiation from Nanostructures Coupled to Chiral Films, *Phys. Rev. Appl.* **17**, 034005 (2022).
- [5] N. Hisamoto, T. Ueda, K. Sawada, and S. Tomita, Observation of asymmetric electromagnetic field profiles in chiral metamaterials, *Phys. Rev. B* **97**, 085105 (2018).
- [6] X. Mu, L. Hub, Y. Cheng, Y. Fang, and M. Suna, Chiral surface plasmon enhanced chiral spectroscopy: principles and applications, *Nanoscale* **13**, 581 (2021).
- [7] A. O. Govorov, Z. Fan, P. Hernandez, J. M. Slocik, and R. R. Naik, Theory of circular dichroism of nanomaterials comprising chiral molecules and nanocrystals: plasmon enhancement dipole interactions, and dielectric effects, *Nano Lett.* **10**, 1374 (2010).
- [8] W. Liu, Z. Zhu, K. Deng, Z. Li, Y. Zhou, H. Qiu, Y. Gao, S. Che, and Z. Tang, Gold nanorod@chiral mesoporous silica core-shell nanoparticles with unique optical properties, *J. Am. Chem. Soc.* **135**, 9659 (2013).
- [9] N. A. Abdulrahman, Z. Fan, T. Tonooka, S. M. Kelly, N. Gadegaard, E. Hendry, A. O. Govorov, and M. Kadodwala, Induced chirality through electromagnetic coupling between chiral molecular layers and plasmonic nanostructures, *Nano Lett.* **12**, 977 (2012).
- [10] M. L. Nesterov, X. Yin, M. Schaferling, H. Giessen, and T. Weiss, The role of plasmon-generated near fields for enhanced circular dichroism spectroscopy, *ACS Photonics* **3**, 578 (2016).
- [11] F. J. Garcia de Abajo, Optical excitations in electron microscopy, *Rev. Mod. Phys.* **82**, 211 (2010).
- [12] H. Inui, A. Fujii, K. Tanaka, H. Sakamotoa, and K. Ishizuka, New electron diffraction method to identify the chirality of enantiomeric crystals, *Acta Crystallogr. B* **59**, 802 (2003).

- [13] C. S. Allen, C. Zhang, G. Burnell, A. P. Brown, J. Robertson, and B. J. Hickey, A review of methods for the accurate determination of the chiral indices of carbon nanotubes from electron diffraction patterns, *Carbon* **49**, 4961 (2011).
- [14] P. Schattschneider, S. Rubino, C. Hebert, J. Rusz, J. Kunes, P. Novak, E. Carlino, M. Fabrizioli, G. Panaccione, G. Rossi, *et al.*, Detection of magnetic circular dichroism using a transmission electron microscope, *Nature* **441**, 486 (2006).
- [15] P. Schattschneider, M. Stöger-Pollach, S. Rubino, M. Sperl, C. Hurm, and Josef Zwec, Detection of magnetic circular dichroism on the two-nanometer scale, *Phys. Rev. B* **78**, 104413 (2008).
- [16] J. Verbeeck, H. Tian, and P. Schattschneider, Production and application of electron vortex beams, *Nature* **467**, 301 (2010).
- [17] K. Y. Bliokh, I. P. Ivanov, G. Guzzinati, L. Clark, R. Van Boxem, A. Béché, R. Juchtmans, M. A. Alonso, P. Schattschneider, F. Nori, and J. Verbeeck, Theory and applications of free-electron vortex states, *Phys. Rep.* **690**, 1 (2017).
- [18] R. Juchtmans and J. Verbeeck, Orbital angular momentum in electron diffraction and its use to determine chiral crystal symmetries, *Phys. Rev. B* **92**, 134108 (2015).
- [19] R. Juchtmans, A. Beche, A. Abakumov, M. Batuk, and J. Verbeeck, Using electron vortex beams to determine chirality of crystals in transmission electron microscopy, *Phys. Rev. B* **91**, 094112 (2015).
- [20] A. Asenjo-Garcia and F. J. García de Abajo, Dichroism in the Interaction between Vortex Electron Beams, Plasmons, and Molecules, *Phys. Rev. Lett.* **113**, 066102 (2014).
- [21] B. Barwick, D. J. Flannigan, and A. H. Zewail, Photon-induced near-field electron microscopy, *Nature* **462**, 902 (2009).
- [22] S. T. Park, M. Lin, and A. H. Zewail, Photon-induced near-field electron microscopy (PINEM): Theoretical and experimental, *New J. Phys.* **12**, 123028 (2010).
- [23] G. M. Vanacore, G. Berruto, I. Madan, E. Pomarico, P. Biagioni, R. J. Lamb, D. McGrouther, O. Reinhardt, I. Kaminer, B. Barwick, H. Larocque, V. Grillo, E. Karimi, F. J. Garcia de Abajo, and F. Carbon, Ultrafast generation and control of an electron vortex beam via chiral plasmonic near fields, *Nat. Mater.* **18**, 573 (2019).
- [24] T. R. Harvey, J.-W. Henke, O. Kfir, H. Lourenco-Martins, A. Feist, F. J. Garcia de Abajo, and Claus Roper, Probing chirality with inelastic electron-light scattering, *Nano Lett.* **20**, 4377 (2020).
- [25] T. Gruner and D.-G. Welsch, Green-function approach to the radiation-field quantization for homogeneous and inhomogeneous Kramers-Kronig dielectrics, *Phys. Rev. A* **53**, 1818 (1996).
- [26] S. Scheel and S. Y. Buhmann, Macroscopic quantum electrodynamics—concepts and applications, *Acta Phys. Slovaca* **58**, 675 (2008).
- [27] S. Y. Buhmann, D. T. Butcher, and S. Scheel, Macroscopic quantum electrodynamics in nonlocal and nonreciprocal media, *New J. Phys.* **14**, 083034 (2012).
- [28] D. T. Butcher, S. Y. Buhmann, and S. Scheel, Casimir-Polder forces between chiral objects, *New J. Phys.* **14**, 113013 (2012).

- [29] A. B. Hayun, O. Reinhardt, J. Nemirovsky, A. Karnieli, N. Rivera, and I. Kaminer, Shaping quantum photonic states using free electrons, *Sci. Adv.* **7**, eabe4270 (2021).
- [30] A. Karnieli, N. Rivera, A. Arie, and I. Kaminer, The coherence of light is fundamentally tied to the quantum coherence of the emitting particle, *Sci. Adv.* **7**, eabf8096 (2021).
- [31] O. Kfir, Entanglements of Electrons and Cavity Photons in the Strong-Coupling Regime, *Phys. Rev. Lett.* **123**, 103602 (2019).
- [32] L. H. Ford, Electromagnetic vacuum fluctuations and electron coherence, *Phys. Rev. D* **47**, 5571 (1993).
- [33] J.-T. Hsiang and D.-S. Lee, Influence on electron coherence from quantum electromagnetic fields in the presence of conducting plates, *Phys. Rev. D* **73**, 065022 (2006).
- [34] P. Schattschneider and S. Löffler, Entanglement and decoherence in electron microscopy, *Ultramicroscopy* **190**, 39 (2018).
- [35] C. Mechel, Y. Kurman, A. Karnieli, N. Rivera, A. Arie, and I. Kaminer, Quantum correlations in electron microscopy, *Optica* **80**, 70 (2021).
- [36] C. W. Johnson, A. E. Turner, F. J. García de Abajo, and B. J. McMorran, Inelastic Mach-Zehnder Interferometry with Free Electrons, *Phys. Rev. Lett.* **128**, 147401 (2022).
- [37] N. Rivera and I. Kaminer, Light–matter interactions with photonic quasiparticles, *Nat. Rev. Phys.* **2**, 538 (2020).
- [38] V. Di Giulio and F. J. García de Abajo, Electron diffraction by vacuum fluctuations, *New J. Phys.* **22**, 103057 (2020).
- [39] F. J. García de Abajo and V. Di Giulio, Optical excitations with electron beams: Challenges and opportunities, *ACS Photonics* **8**, 945 (2021).
- [40] A. Hayat, J. P. B. Mueller, and F. Capasso, Lateral chirality-sorting optical forces, *Proc. Natl. Acad. Sci.* **112**, 13190 (2015).
- [41] Y. Shi, T. Zhu, T. Zhang, A. Mazzulla, D. P. Tsai, W. Ding, A. Q. Liu, G. Cipparrone, J. J. Sáenz, C.-W. Qiu, *et al.*, Chirality-assisted lateral momentum transfer for bidirectional enantioselective separation, *Light Sci. Appl.* **9**, 62 (2020).
- [42] Y. Chen, C. Zhao, Y. Zhang, and C.-W. Qiu, Integrated molar chiral sensing based on high- Q metasurface, *Nano Lett.* **20**, 8696 (2020).
- [43] A. Orchowski, W. D. Rau, and H. Lichte, Electron Holography Surmounts Resolution Limit of Electron Microscopy, *Phys. Rev. Lett.* **74**, 399 (1995).
- [44] P. L. Potapov, J. Verbeeck, P. Schattschneider, H. Lichte, and D. van Dyck, Inelastic electron holography as a variant of the Feynman thought experiment, *Ultramicroscopy* **107**, 559 (2007).
- [45] S. Frabboni, A. Gabrielli, G. Gazzadi, F. Giorgi, G. Matteucci, G. Pozzi, N. S. Cesari, M. Villa, and A. Zoccoli, The Young-Feynman two-slits experiment with single electrons: Build-up of the interference pattern and arrival-time distribution using a fast-readout pixel detector, *Ultramicroscopy* **116**, 73 (2012).
- [46] S. Frabboni, G. Gazzadi, V. Grillo, and G. Pozzi, Elastic and inelastic electrons in the double-slit experiment: A variant of Feynman’s which-way set-up, *Ultramicroscopy* **154**, 49 (2015).
- [47] P. Shekhar, M. Malac, V. Gaind, N. Dalili, A. Meldrum, and Z. Jacob, Momentum-resolved electron energy loss spectroscopy for mapping the photonic density of states, *ACS Photonics* **4**, 1009 (2017).
- [48] H. T. Dung, L. Knoll, and D.-G. Welsch, Three-dimensional quantization of the electromagnetic field in dispersive and absorbing inhomogeneous dielectrics, *Phys. Rev. A* **57**, 3932 (1998).
- [49] R. M. Wilcox, Exponential operators and parameter differentiation in quantum physics, *J. Math. Phys.* **8**, 962 (1967).